DOE/PC/89783--T12
(DE94018038)
Distribution Category UC-108

Final Report to US Department of Energy

Project title: "Fundamental Studies of Catalytic Processing of Synthetic Liquids"

Project number: DE-FG22-89PC89783

Principal Investigator: Prof. Philip R. Watson
Department of Chemistry and Center for Advanced Materials Research
Oregon State University
Gilbert Hall 153
Corvallis, OR 97331-4003

(503)-737-2081

Date of report: 6/15/94

DISCLAIMER

DISCLAIMER

Portions of this document may be illegible in electronic image products. Images are produced from the best available original document.

TABLE OF CONTENTS

ABSTRACT

Liquids derived from coal contain relatively high amounts of oxygenated organic compounds, mainly in the form of phenols and furans that are deleterious to the stability and quality of these liquids as fuels. HDO using Mo/W sulfide catalysts is a promising method to accomplish this removal, but our understanding of the reactions occurring on the catalyst surface during HDO is very limited. Rather than attempting to examine the complexities of real liquids and catalysts we have adopted an approach here using model systems amenable to surface-sensitive techniques that enable us to probe in detail the fundamental processes occurring during HDO at the surfaces of well-defined model catalysts. The results of this work may lead to the development of more efficient, selective and stable catalysts.

Above a S/Mo ratio of about 0.5 ML, furan does not adsorb on sulfided Mo surfaces; as the sulfur coverage is lowered increasing amounts of furan can be adsorbed. Temperature-programmed reaction spectroscopy (TPRS) reveals that C-H, C-C and C-O bond scission occurs on these surfaces. Auger spectra show characteristic changes in the nature and amount of surface carbon. Comparisons with experiments carried out with CO, H_2 and alkenes show that reaction pathways include - direct abstraction of CO at low temperatures; cracking and release of hydrogen below its normal desorption temperature; dehydrogenation of adsorbed hydrocarbon fragments; recombination of C and O atoms and dissolution of carbon into the bulk at high temperatures. Performing the adsorption or thermal reaction in 10^{-5} torr of hydrogen does not change the mode of reaction significantly.

1. INTRODUCTION

1.1 Background

It is likely that liquid fuel producers will soon have to process increasing amounts of synthetic feedstocks that will contain far higher levels of molecules containing S, N and O atoms than those in traditionally available petroleum stocks. The problems associated with S and N poisoning of downstream catalysts, and environmental concern to limit harmful SO_2 and NO_x emissions, have stimulated extensive research programs into the removal of these species from fuels. The comparative lack of interest in oxygen removal can probably be traced to the low oxygen level found in commercial crude oils, and the fact that the heteroatom can be removed in a relatively innocuous form as water.

However, synthetic fuels derived from fossil or biomass sources contain far higher amounts of oxygen. Furthermore, levels of oxygen in these synfuels can be an order of magnitude higher than those of S and N, and can lead to a unique set of processing problems. Such synthetic liquids tend to be unstable, becoming dark-colored and forming deposits on exposure to air. Hence O-removal is a necessary step in the production of stable commercial synfuels, and catalytic processing offers a viable solution.

Hydrodesulfurization (HDS) and hydrodenitrogenation (HDN) reactions occur simultaneously with hydrodeoxygenation (HDO) during catalytic hydroprocessing of fuels. All the heteroatom-removal reactions are catalyzed by Mo or W, usually as sulfides, and most often promoted with Co or Ni. There has been extensive research into the catalytic HDS [1-4] and HDN [1,5,6] reactions. Some reaction networks are understood in detail, and at least for HDS, the nature

of the active sites on the surface of the catalyst is becoming much clearer.

Our knowledge of HDO chemistry is much less well developed [7]. Only a small number of model compound studies over supported catalysts have been reported to establish the reaction networks, and the effects of interactions between HDO and competing HDS and HDN processes.

In contrast to the situation with HDS (discussed later), there appear to be no attempts to bring the tools of surface chemistry to bear on HDO catalysis. This research proposal will be the first attempt to provide a surface chemical viewpoint on HDO catalysis. It will focus on a number of well-defined goals that attempt to probe the origins of reactivity and selectivity of the HDO reaction:

- to describe the bonding of O-compounds at different types of surface site
- to find the relative importance of C-O bond-breaking and hydrogenation on these different types of sites
- to understand how adsorption and reaction depend on the structure of the reactant
- to determine to what extent HDO reactions are affected by competitive adsorption of other reactants and products

Achieving the above goals is important in developing a detailed understanding of HDO catalysis. With atomic-level descriptions of the surface chemistry, we can then apply them to:

- improve catalyst activity and selectivity by tailoring the concentration of active sites of known characteristics
- predict the response of catalysts to new feedstocks from a knowledge of the effect of reactant structure

and hence,

- impact the design of new catalysts for processing synthetic feeds

Because of the atomic-level detail that fundamental surface science investigations reveal, such model studies can play a significant role in understanding the processes occurring at the active sites

on a catalyst's surface. This is only true, however, if we have some assurance that the model surface and reactants used are truly representative of real materials. In addition, we must address the issue of the transferability of results obtained under conditions far removed from those of industrial practice.

True hydroprocessing catalysts are complex multicomponent systems, involving supports and promoters. Hence, it is often difficult to untangle the elementary steps occurring during catalysis. The model surface chemistry approach developed in this proposal emphasizes uncoupling the surface chemistry from the complexity of the promoted supported catalysts by making simple single crystal models, which possess predominantly only one type of active site. We have attempted to make these model catalysts reproduce as closely as possible the chemical nature of true HDO catalysts. In addition, we have tried to select simple model reactants that provide the necessary essential chemistry with sufficient simplicity to enable us to obtain a detailed understanding.

Reducing the problem to one involving a simple but representative model allows us to take advantage of surface sensitive techniques. By their nature, however, surface science experiments take place in a low-pressure environment, unless very specialized apparatus is available. In such a case, how can we relate the results obtained to catalysis performed at much higher pressures?

There are two arguments that support the contention that surface science experiments on HDO catalysis, carried out at sub-torr pressures, can yield meaningful information for processes that take place at 1000's of psi of hydrogen.

The first argument is that in HDO reactions the significant quantity is not the absolute hydrogen pressure, but rather the surface concentration of hydrogen relative to that of the reactant. Under the usual practical conditions, the reactant is probably present in high concentration at the surface, and adsorbs more strongly than hydrogen. This is particularly so at the elevated temperatures used to get a sufficiently high reaction rate. Hence, in typical catalytic practice, a high hydrogen

pressure is necessary to force hydrogen onto the surface. In contrast, under surface science experimental conditions, the surface concentration of reactant can be closely controlled to a relatively small fraction of a monolayer. As a result, a high hydrogen/reactant ratio can be maintained on the surface by i) keeping surface adsorption sites free for hydrogen to adsorb and ii) using a hydrogen atmosphere that is sufficient to saturate the surface with hydrogen yet allow for surface analysis e.g. 10^{-5} torr.

The second argument is that there are a number of examples in the literature where rate measurements, and product distributions, measured under idealized surface science conditions compare very well with those found under high-pressure "real" conditions - the so-called "pressure-gap" and "complexity-gap" have been bridged.

1.2 Catalytic HDO Studies

The amount and type of O-containing molecules found in different synfuels can vary depending upon the feedstock and liquefaction process. However, detailed component identification by GC-MS methods has revealed that the major O-compounds that resist processing in fuels derived from coal and oil-shales are phenolic or furanic [8].

Furimsky [7] has summarized the results of a number of studies that followed the fate of O-compounds in full fossil-derived liquids. In order to obtain a better grasp of kinetics and reaction networks, a number of investigators have performed model compound studies over Co-Mo and Ni-Mo catalysts, shown in Table 1.1. The results of these studies have provided some interesting insights into the reaction networks, but only scanty information on events occurring on the catalyst surface during reaction.

Two themes recur in HDO studies of the reaction networks of model compounds. One concerns the crucial role that the surface concentration of hydrogen can play in product selectivity, while the other focusses on the steric effects induced by different structures in the reactant.

Table 1.1 Selected model compound studies of HDO over typical catalysts.

Model compound	Catalyst	Ref.
Furan	$Co\text{-}Mo/Al_2O_3$	14
Tetrahydrofuran (THF)	$Co\text{-}Mo/Al_2O_3$	15
Benzofuran (BF)	$Co\text{-}Mo/Al_2O_3$	19,24
Dibenzofuran (DBF)	$Co\text{-}Mo/Al_2O_3$ $Ni\text{-}Mo/Al_2O_3$ $Ni\text{-}W/Al_2O_3$	12,18 9-12,24 13
Diphenylether	$Co,Ni\text{-}Mo/Al_2O_3$	23
Cresols	$Co\text{-}Mo/Al_2O_3$ $Ni\text{-}Mo/Al_2O_3$ $Ni\text{-}W/Al_2O_3$	13,17,21 12,16 13
o-ethylphenol	$Co\text{-}Mo/Al_2O_3$	18,21

The most obvious role of surface hydrogen in selectivity is in determining the relative importance of C-O bond scission reactions to those leading to ring hydrogenation. Krishnamurty et al [24] have performed a detailed study of the product distribution for HDO of benzofuran (DBF). The reaction network they propose (Figure 1.1) illustrates the role of available hydrogen. At high pressures, one ring is hydrogenated to a o-cyclohexylphenol intermediate (Route 1a). Subsequent O-extraction can give either predominantly bicyclohexyl (Route 1c,d), or at lower H-pressures, phenylcyclohexane (Route 1e). Under conditions where surface hydrogen is less abundant, Route 2, and possibly direct extrusion via Route 3, leading to more aromatic products, become more important.

The role of surface hydrogen is also manifested in the selectivity to HDO of a saturated

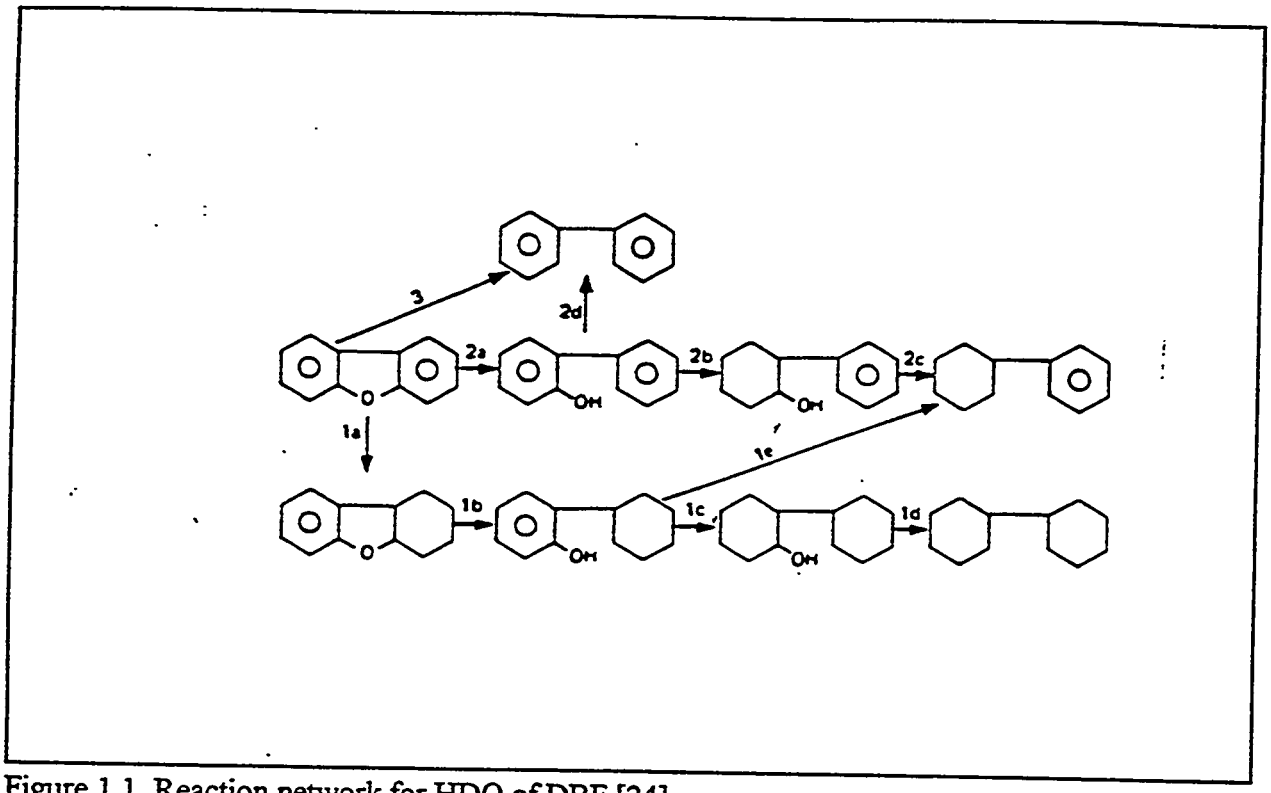

Figure 1.1 Reaction network for HDO of DBF [24].

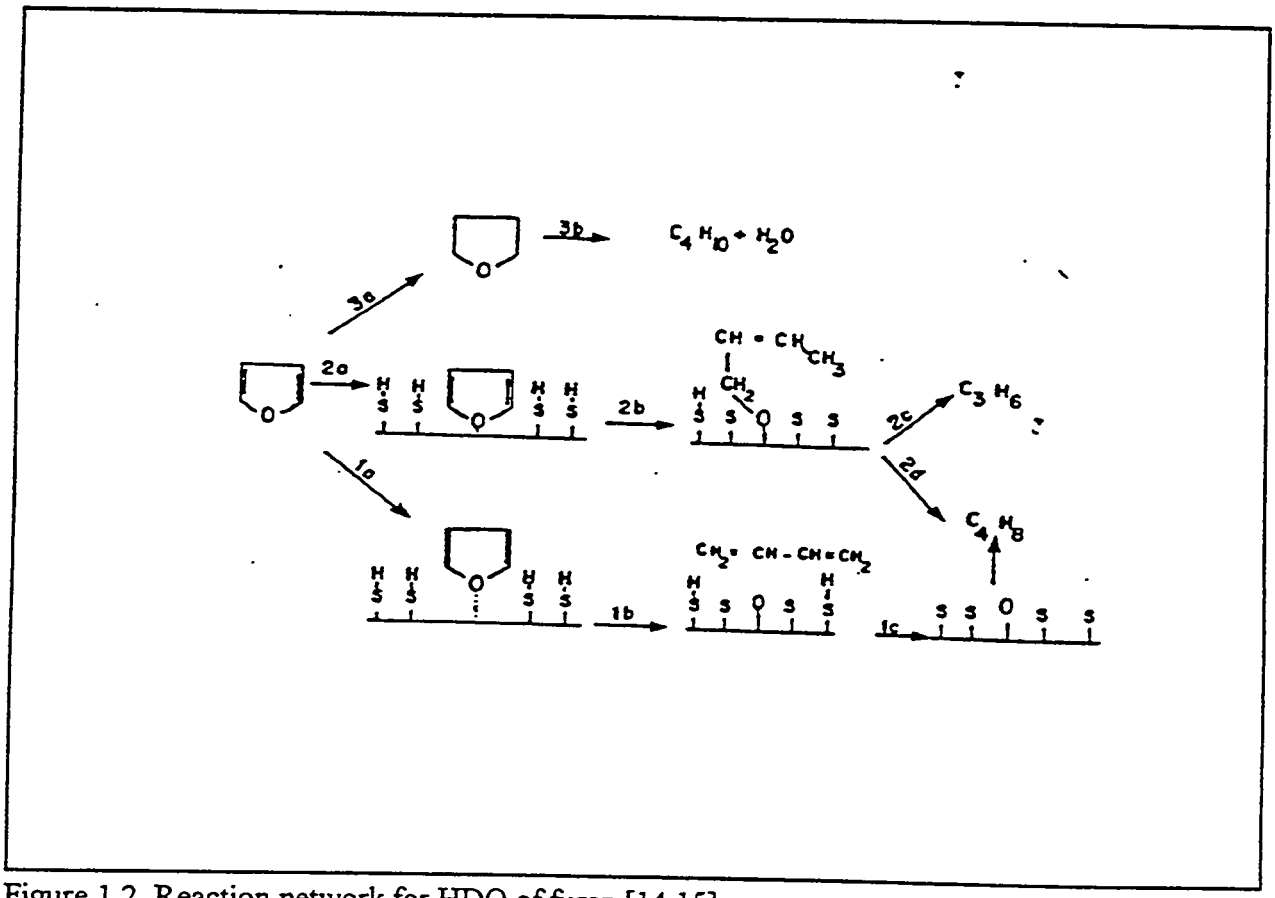

Figure 1.2. Reaction network for HDO of furan [14,15].

reactant. Thus, Furimsky [14,15] found that for THF, O-extraction took place to a small extent even in the absence of hydrogen, to give butadiene. This was thought to arise from an internal shift of H atoms of the THF molecule (Figure 1.2). Under 1 atm of hydrogen, THF gave predominantly 1-butene over the sulfided catalyst. This was attributed to much more efficient H-transfer of adsorbed hydrogen on the catalyst surface, leading to ring opening.

Another theme that runs through the literature concerning HDO mechanisms is that the structure of the reactant can have dramatic effects on product yield and distribution. Such effects are typically labelled as steric in nature. For example, o-alkylphenols are more resistant to typical HDO processing than m-alkylphenols [19]. This has been attributed to steric hindrance restricting the access of surface hydrogen to the C-OH bond. Similar hindrance is thought to account for the high degree of ring hydrogenation seen in the HDO of dibenzofuran (DBF) [7], relative to the HDS of dibenzothiophene [1]. The smaller O heteroatom may be more hindered in accessing the surface hydrogen, thus forcing C-O bond rupture to occur only after extensive ring hydrogenation.

Many workers have noted that the reactivity and selectivity of HDO for a particular compound depend markedly on the catalyst, on its preparation and pretreatment. Thus, Furimsky [14,15] found that for the HDO of furan under 1 atm. of hydrogen, a sulfided Co-Mo catalyst was over 6 times more active than the reduced form. Other authors have reported beneficial effects of presulfiding [9] and the dramatic effects of different preparative methods [7]. However, such effects may differ for different reactants and experimental conditions; in the case of high-pressure HDO of 1-naphthol, Gates et al [20,22] found that sulfidation of their catalyst reduced activity.

There appear to be no reported studies directly concerned with spectroscopic measurements of the nature of the catalytically active surface, or of surface events occurring during HDO reactions. In the absence of direct experimental data concerning the adsorption and reaction of O-containing molecules, many workers have relied upon extrapolation from the better-developed HDS literature.

Here a large body of catalytic and IR, EXAFS and other studies [1-5] have lead to the proposal that adsorption of an S-molecule is at an anion vacancy in an $Mo(W)S_2$ type of layer on the catalyst surface. These vacancies probably are at edge sites and are possibly associated with a promoter species.

Most workers assume that HDO reactions occur on sulfided catalysts at similar locations to those involving HDS. The same catalysts are often efficient for both types of reaction, and both reactions are similarly inhibited by nitrogen bases [7]. It seems unclear how many types of active site are involved. Suggestions include HDO taking place at the same site as ring hydrogenation [21], or at separate, but similar, anion vacancy sites [22].

1.3 Relevant surface science literature

The methods of surface science have contributed very valuable information on surface structure, bonding and reactions in a number of area of catalysis. However, the literature does not contain studies of the adsorption and reaction of representative HDO reactants with model surfaces involving the catalytically active metals Mo and W. A limited study on clean Ru(0001) [34] found that furan decomposed on heating.

We can turn to HDS-based studies for guidance. HDS reactions have been observed over the model surface of Mo(100) at a hydrogen pressure of 1 atm [25,26]. Several authors have studied the interaction of thiophenes with Mo(100) [27-29], Mo(110) [30,31] and W(211) [32] under ultra-high vacuum (UHV) conditions. These studies have focussed on the interaction of thiophene and tetrahydrothiophene (THT) at low pressures with clean metal surfaces, and with surfaces containing oxygen, carbon or sulfur. Behavior on these three surfaces seems to be quite similar, suggesting that the surface geometry may not be a deciding factor for these molecules under this particular set of experimental conditions.

Under UHV conditions thiophene decomposes on the clean surfaces, but sulfur adlayers

inhibit the decomposition reactions. It seems likely that the mode of bonding of thiophene changes from parallel pi-bonded to an upright orientation as the coverage of the surface with reactant is increased. The high electron-density at the 2-position in thiophene [33] appears to facilitate an electrophilic reaction in which the C-H bond α to the S atom is broken resulting in an upright adsorption mode bonded through a C atom. High-resolution electron energy loss (HREELS) spectra [29] suggest that bonding occurs through a metallacycle species on clean Mo(100).

THT undergoes HDS under UHV conditions on both W(211) [31] and Mo(110) [31]. In this case, the non-aromatic molecule adsorbs through the S atom, followed by C-S scission to form an intermediate thiolate. In fact THT and butanethiol appear to react through a common butyl thiolate intermediate bound directly through S.

1.4 References

1. "Chemistry of Catalytic Processes", B.C. Gates, J.R. Katzer, and G.C.A. Schuit, McGraw-Hill, New York, 1979.
2. E. Furimsky, Catal. Rev. - Sci. Eng., 22 (1980) 371.
3. R.R. Chianelli, in "Catalysis and Surface Science", Chemical Industries 21, ed. H. Heinemann and G.A. Somorjai, Dekker, 1985, p. 61.
4. H. Topsoe and B.S. Clausen, ibid, p. 95.
5. J.R. Katzer and R. Sivasubramaian, Catal. Rev. - Sci. Eng., 20 (1979) 155.
6. J. Sonnemans and P. Mars, J. Catal. 31 (1973) 209.
7. E. Furimsky, Catal. Rev. - Sci. Eng., 25 (1983) 421.
8. a) E. Furimsky, J.A. McPhee, L. Vancea, L.A. Ciavaglia, and B.N. Landi, Fuel, 62 (1983) 395.

   b) M. Novotny, J.W. Strand, S.L. Smith, D. Wiesler, and F.J. Schwende, Fuel, 60 (1981) 213.
9. S. Krishnamurthy, S. Panvelker, and Y.T. Shah, AIChE J., 27 (1981) 994.

10. R. Badilla-Ohlbaum, K.C. Pratt, and D.L. trimm, Fuel, 58 (1979) 309.

11. S. Kuruppannasamy, K. Narayanan and, C.N. Pillay, J. Catal. 63 (1980) 433.

12. T.O. Mitchell, Coal Processing Technology, Vol. 6, 1980, p.28.

13. R.J. Bertolacini, J.M. Forgac, D.M. Kim, R.J. Pellet, and K.K. Robinson, "Chemistry and Uses of Molybdenum", in Proc. Third Int. Conf., Climax Molydenum Co.

14. E. Furimsky, Applied Catal. 6 (1983) 159.

15. E. Furimsky, Ind. Eng. Chem. Prod. Res. Dev., 22 (1983) 31.

16. R.K.M.R. Kallury, W.M. Restivo, T.M. Tidwell, D.G.B. Boocock, A. Crimi, and J. Douglas, J. Catal. (1985) 535.

17. O. Odebunmi, Ph. D. Thesis, Princeton University (1981).

18. C-L. Li and D.F. Ollis, J. Catal. 87 (1984) 325.

19. L.D. Rollman, J. Catal., 46 (1977) 243.

20. C-L. Li, Z-R. Xu, Z-A. Cao, and B.C. Gates, AIChE J., 31 (1985) 170.

21. H. Weigold, Fuel 61 (1982) 1021.

22. M.W. Vogelzang, C-L. Li, G.C.A. Schuit, B.C. Gates, and L. Petrakis, J. Catal., 84 (1983) 170.

23. J. Shabtai, N.K. Nag, and F.E. Massoth, J. Catal., 104 (1987) 413.

24. S. Krishnamurty, S. Panvelker, and Y.T. Shah, AIChE J., 27 (1981) 994.

25. A.J. Gellman, D. Neiman, and G.A. Somorjai, J. Catal. 107 (1987) 92.

26. A.J. Gellman, M.E. Bussell, and G.A. Somorjai, J. Catal. 107 (1987) 103.

27. A.J. Gellman, M.H. Farias, M. Salmeron, and G.A. Somorjai, Surface Sci. 136 (1984) 217.

28. D.G. Kelly, M. Salmeron and G.A. Somorjai, Surface Sci. 175 (1986) 465.

29. F. Zaera, E.B. Kollin, and J.L Gland, Surface Sci. 184 (1987) 75.

30. J.T. Roberts and C.M. Friend, J. Am. Chem. Soc. 108 (1986) 7204.

31. J.T. Roberts and C.M. Friend, Surface Sci. 186 (1987) 201.

32. R.E. Preston and J.B. Benziger, J. Phys. Chem. 89 (1985) 5010.

33. S. Kolboe and C.H. Amberg, Can. J. Chem. 44 (1966) 2623.

2. EXPERIMENTAL

The experiments were carried out in an ion-pumped UHV chamber. The base pressure after baking was in the low 10^{-10} torr region. The chamber was equipped with conventional 4-grid LEED/Auger optics (Varian), a quadrupole mass-spectrometer (Ametek) and an in-situ sulfur electrochemical source [1] (produces mainly S_2).

The samples were cut from a single crystal boule of Mo and oriented it to expose either the (100) or (110) crystal face when cut as judged by Laue back-reflection X-ray photographs.. The oriented cut slices were then polished with successive grades of abrasive down to 0.05μ alumina and thoroughly washed. A sample was mounted on an XYZ manipulator that allowed for both heating and cooling, the temperature being monitored with a W/5%Re - W/26%Re thermocouple. In order to acheive the high temperatures necessary to clean Mo without ion-bombardment (up tp 2000K) we employed electron-beam heating (Figure 2.1). For thermal desorption we employed resistive heating controlled by a temperature controller (RHK/HP).

The surfaces were cleaned by cycles of heating for 1 minute in $2x10^{-7}$ torr O_2 at 1000°K followed by a brief 30 second flash to 1800°K. By monitoring the surface composition with Auger electron spectroscopy we found that surface carbon is burned in the oxygen ambient, and the resulting oxides desorb during the high-temperature flash. Sulfur could be deposited sufficient to provide more than a monolayer on the surface. The sample was then carefully annealed at 550K to reduce the

Figure 2.1 Electron beam sample heating assembly

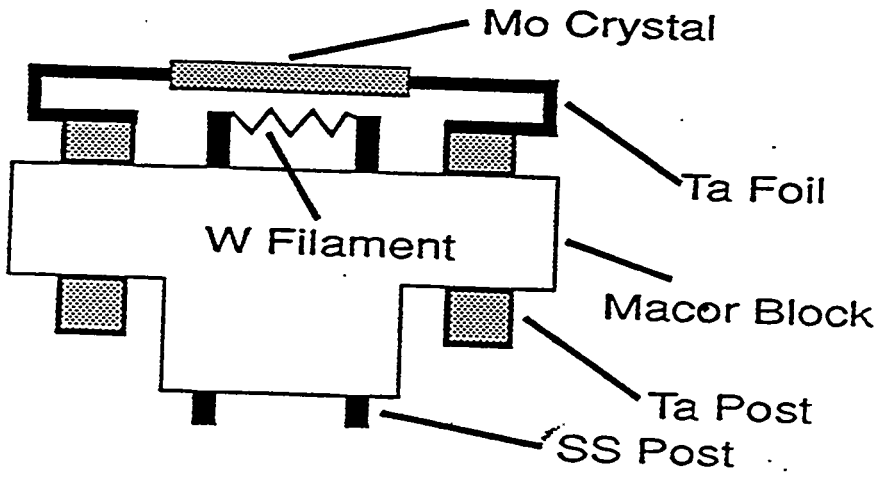

sulfur coverage. This procedure resulted in reasonably sharp LEED patterns at coverages close to those reported in other laboratories [2-5].

1. N.D. Spencer, P.J. Goddard, P.W. Davies, M. Kitson and R.M. Lambert, J. Vac. Sci. Technol. **A1**, 1554 (1983).
2. L. Peralta, Y. Berthier and J. Oudar, Surf. Sci. **55**, 199 (1976).
3. A. Sanchez, J.J. De Miguel, E. Martinez and R. Miranda, Surf. Sci. **171**, 157 (1986).
4. W. Witt and E. Bauer, Ber. Bunsenges. Phys. Chem. **90**, 248 (1986).
5. L. Morales de Garza and L.J. Clarke, J. Phys. C **14**, 5391 (1981).

3. CONSTRUCTING MODEL CATALYST SURFACES

3.1 Sulfur adsorption on the Mo(100) surface

An initial objective of this project was to discover how to reliably and reproducibly produce S overlayers on a Mo(100) surface of known composition. Figure 3.1 shows the raw Auger electron spectroscopy (AES) data that illustrate our ability to make i) a clean Mo surface, free from surface C and O, and ii) using the in-situ electrochemical sulfur source, to cover this surface with a monolayer of S atoms. This sulfur can then be removed in stages by heating as shown in Figure 3.2. After heating to 1800K, a clean S-free surface is recovered.

We can convert raw AES S/Mo signal ratios into surface coverages via a formalism suggested by Salmeron et al [2]:

$$\theta_S = \frac{r^2\,[-Mo(0)^2\alpha]+r\,[Mo(0)S(1)]}{r^2\,[\alpha^2 Mo(0)^2-\alpha Mo(0)^2]+r\,[Mo(0)S(1)-2\alpha Mo(0)S(1)]+S(1)^2}$$

to produce the calibration curve shown in Figure 3.3.

Figure 3.1 AES spectra of a) clean Mo(100) and b) Mo(100) with ~1 ML sulfur

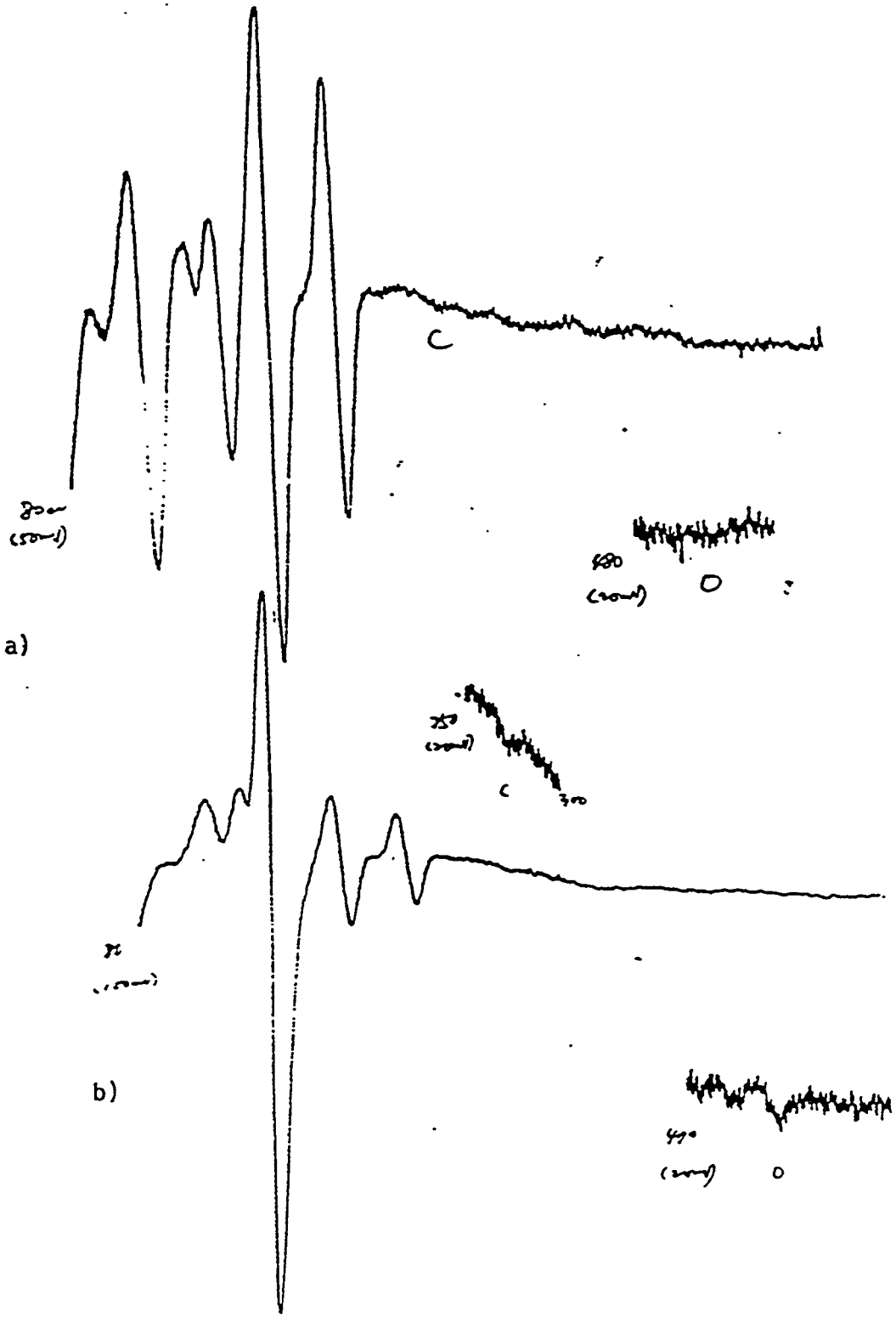

Figutr 3.2 Sulfur desorption from Mo(100)

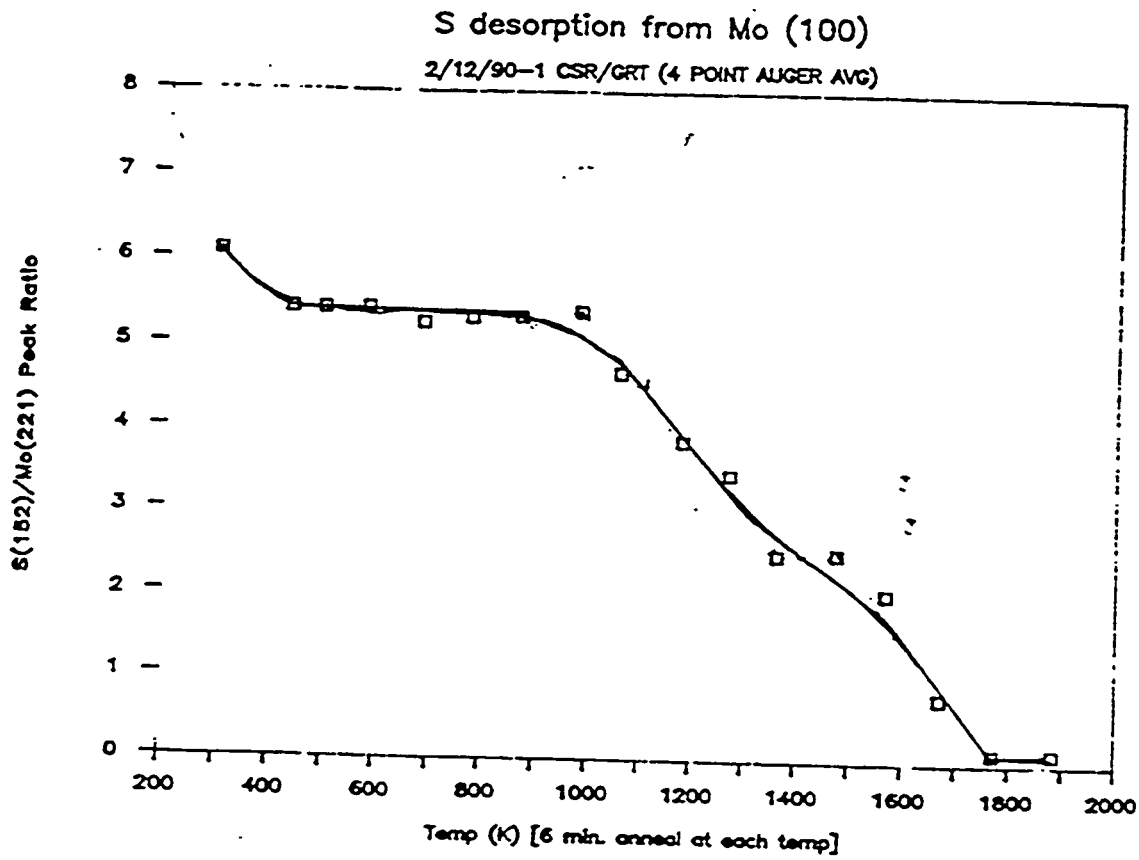

Figure 3.3 Sulfur adsorption on Mo(100) as measured by AES

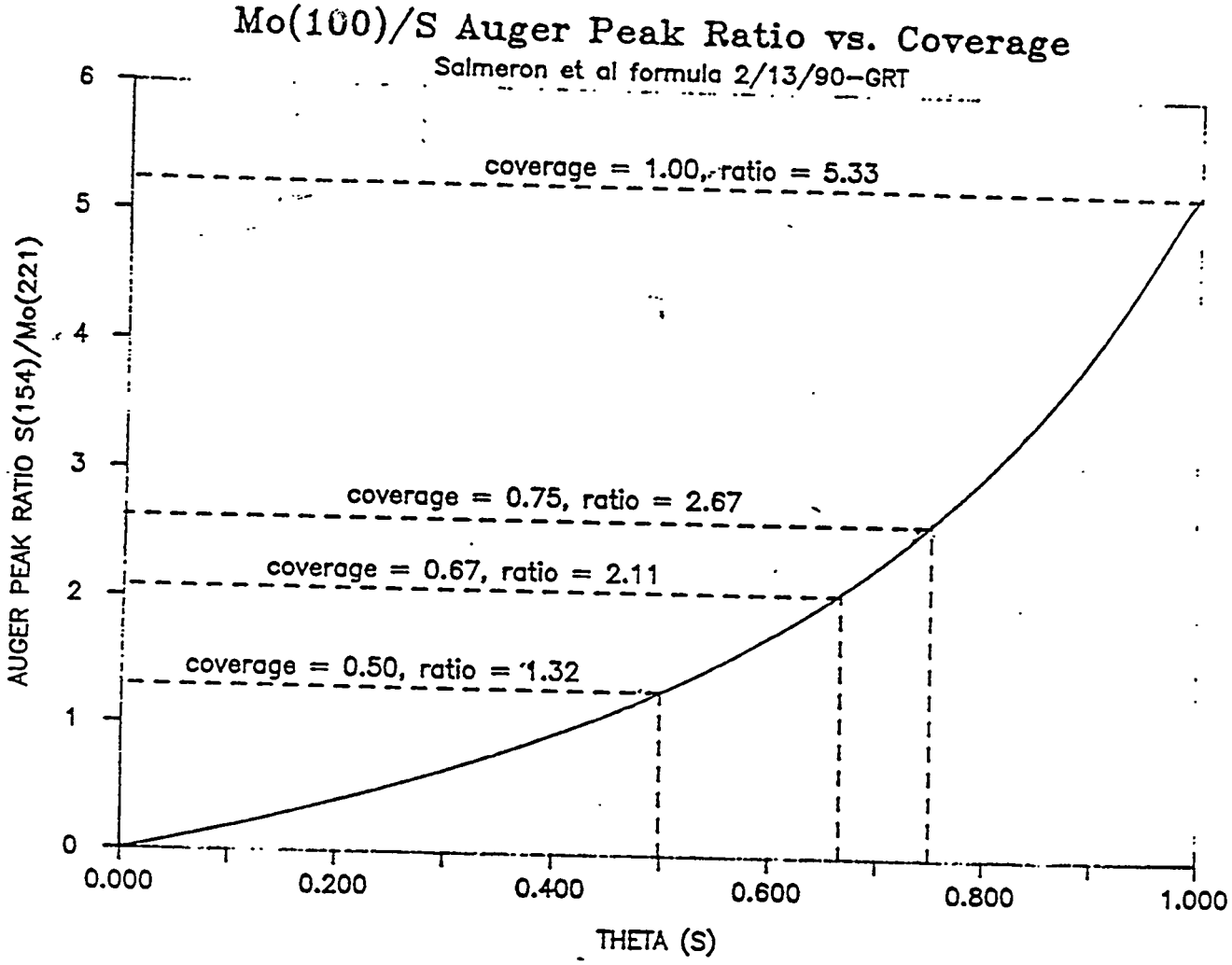

Table 3.1. LEED patterns reported for Mo(100)/S system at various S coverages.

	LEED patterns			
	c(2x2)	(2 -1 1 1)	c(4x2)	p(2x1)
Salmeron et al [2]	0.3 - 0.5	0.54 - 0.69	0.6 - 0.77	0.47 - 0.63
Clark [1]	0.5	0.65	0.8	1.0
Maurice et al [4]	0.5	0.66	0.7 - 0.8	0.8 - 1.0
This work	0.5	0.66	0.8	1.0

We observe a number of ordered surface phases via low-energy electron diffraction (LEED) as a function of surface coverage (Figure 3.4 and Table 3.1). These are in good agreement with previous studies [1-7]; in common with Clarke [1] and Maurice et al [4] we find that the (2x1) LEED patterns are a high coverage phenomenon, rather than relatively low coverage phase as suggested by Salmeron et al [2]. Recent conversations with Salmeron and Somorjai suggest that they now agree with our assignment. From previous studies and experience we can formulate reasonable models for the structure of these surfaces. The likely structures corresponding to the above phases are shown in Figure 5 [1-4]. These structures assume that the top layer Mo atoms are not rearranged upon S adsorption. This assumption is probably untrue, but the displacements are likely to be rather small.

Figure 3.4 LEED pattterns observed at various sulfur coverages on Mo(100)

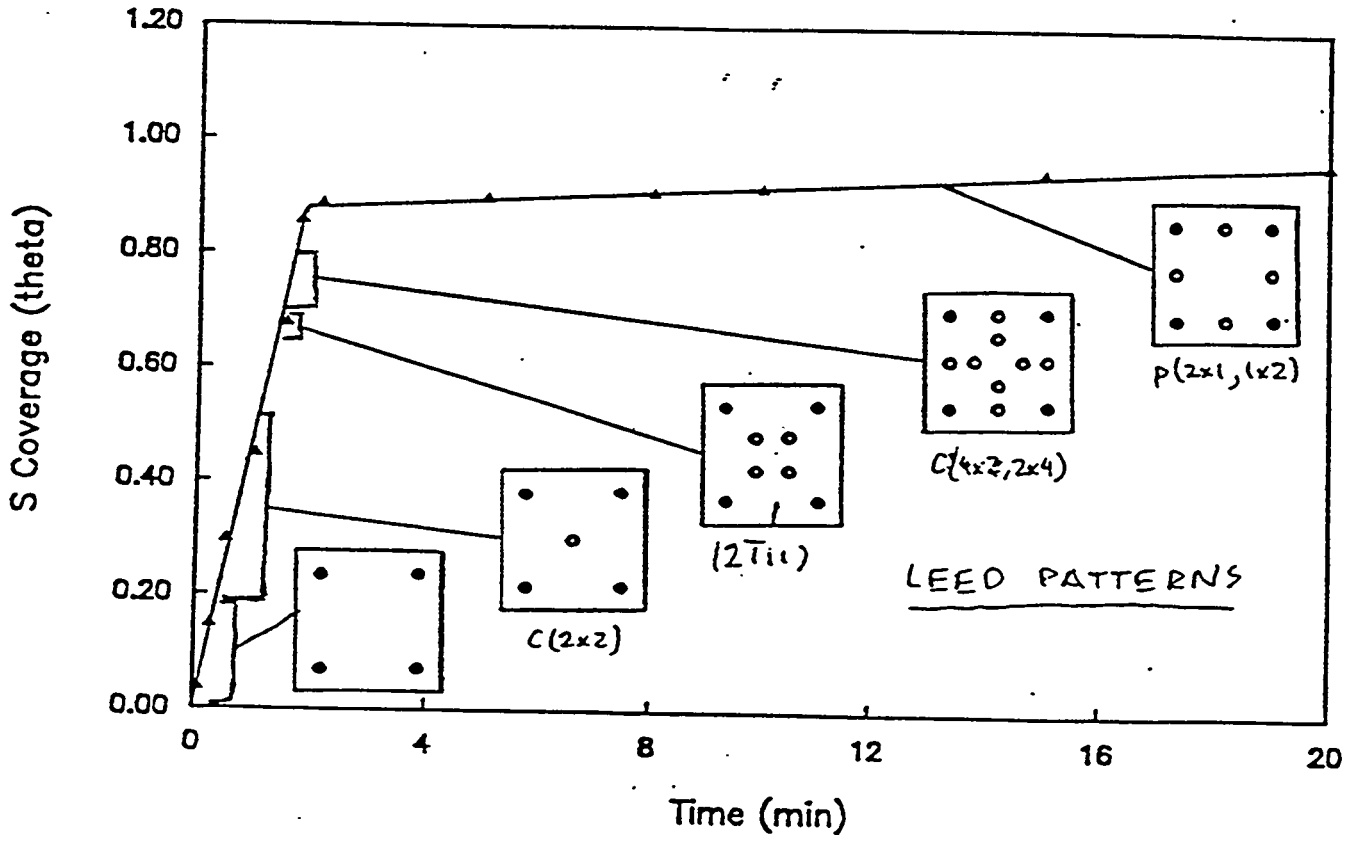

3.2 Sulfur adsorption on the Mo(110) surface

The arrangement of surface atoms at the Mo(110) surface differs from that on Mo(100) - shows the atomic packing is roughly 1.4 times more dense (Figure 3.5). After many heating cycles involving removal of surface carbon with oxygen and high-temperature desorption of Mo oxides we obtained a clean surface with a moderately sharp LEED pattern characteristic of Mo(110). The crystallinity of this surface does not seem to be as good as that of the Mo(100) surface studied previously.

Figure 3.6 shows the variation of S coverage with annealing temperature via a desorption plot. After deposition of S on the surface via an electrochemical cell, the sample was heated to successively higher temperatures and the change in the sulfur Auger signal measured.

The LEED patterns observed for the S/Mo(110) system are not as straightforward as those for the S/Mo(100) and fall into two distinct sets. At high coverages ($\Theta > 0.5$) the patterns observed generally have increasing numbers of superlattice spots in the (110) direction with increasing coverage [5-7]. For our purposes, however, it is of more interest to concentrate on the lower coverages ($\Theta <= 0.5$) which are more likely to produce strong adsorption sites for oxygenates. Fortunately the LEED patterns for this lower coverage region have been well characterized by Sanchez et al [6] and the phase diagram from that work is reproduced in Figure 3.7. At the lowest coverages, a p(2x2) LEED pattern dominates, which has been attributed to S atoms adsorbed in 4-fold sites as shown in Figure 3.8a. Above about 1/3 ML a c(2x2) structure occurs, thought to be due to a more close-packed S arrangement (Figure 3.8b). Above 0.4 ML another structure designated in matrix notation as (2,1,2,-1) is stable below 500K (Figure 3.8c).

Figure 3.5 Comparison of the ideal surfaces of Mo(100) and Mo(110).

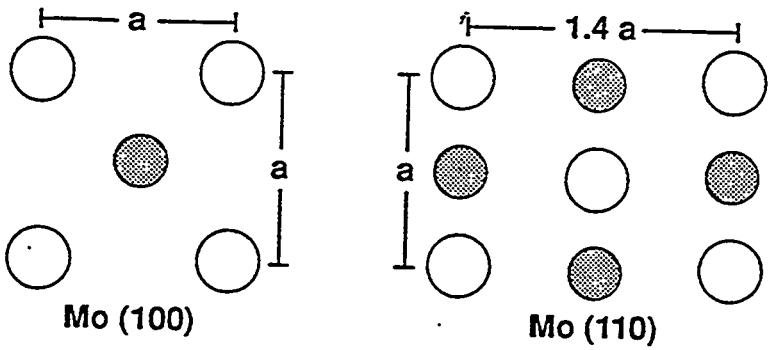

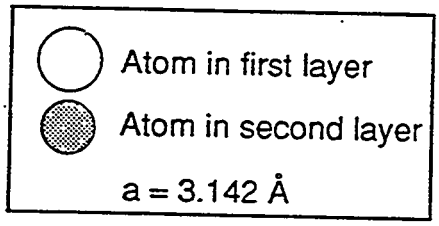

Figure 3.6 S desorption for Mo(110) as measured by AES.

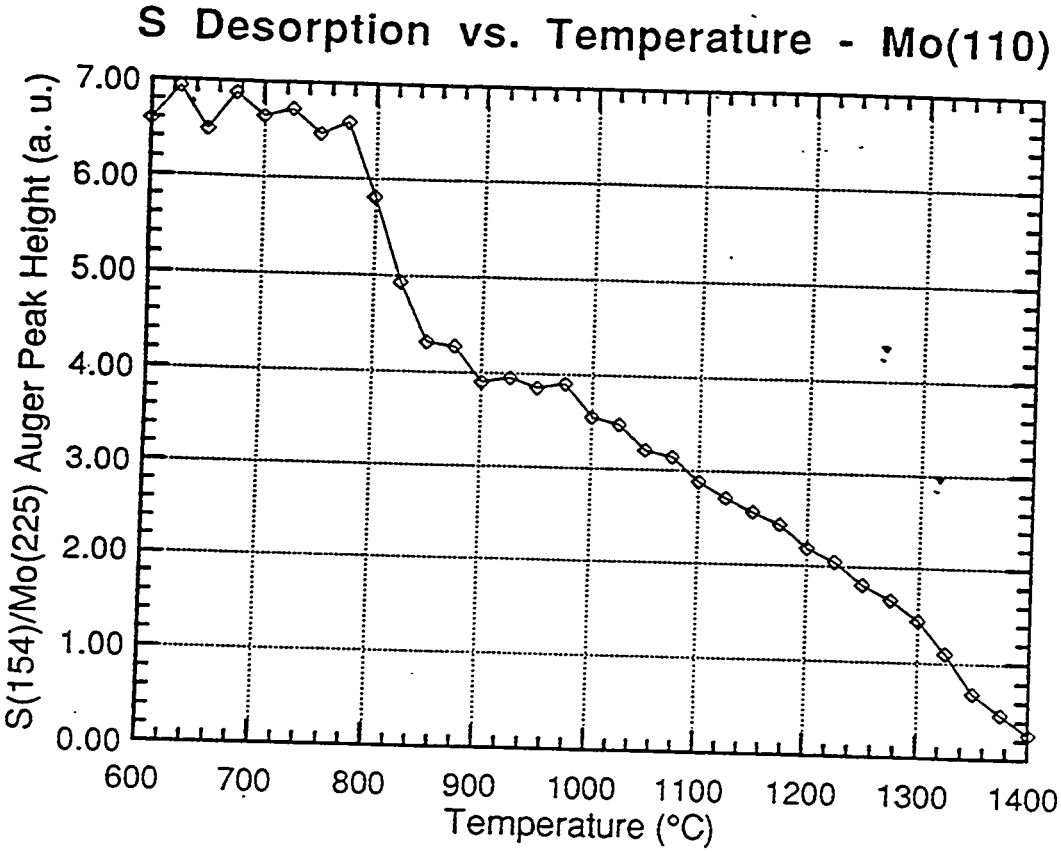

Figure 3.7 Phase diagram of S/Mo(110) system [6].

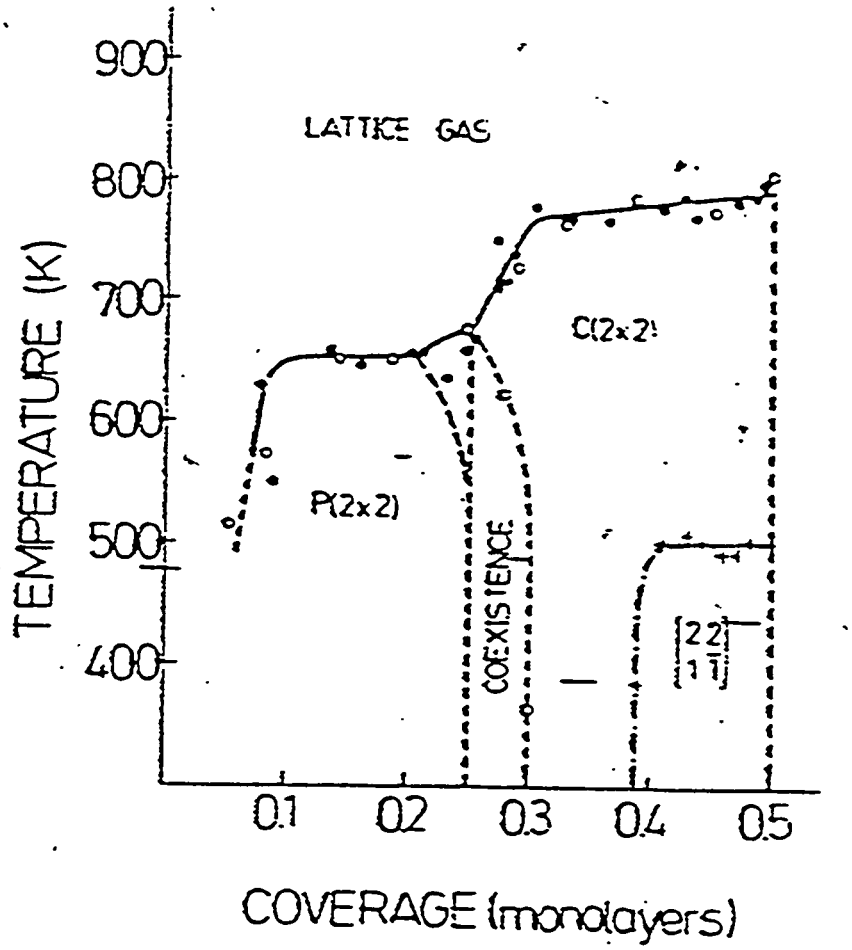

Figure 3.8 LEED patterns and postulated models for S/Mo(110) [6]

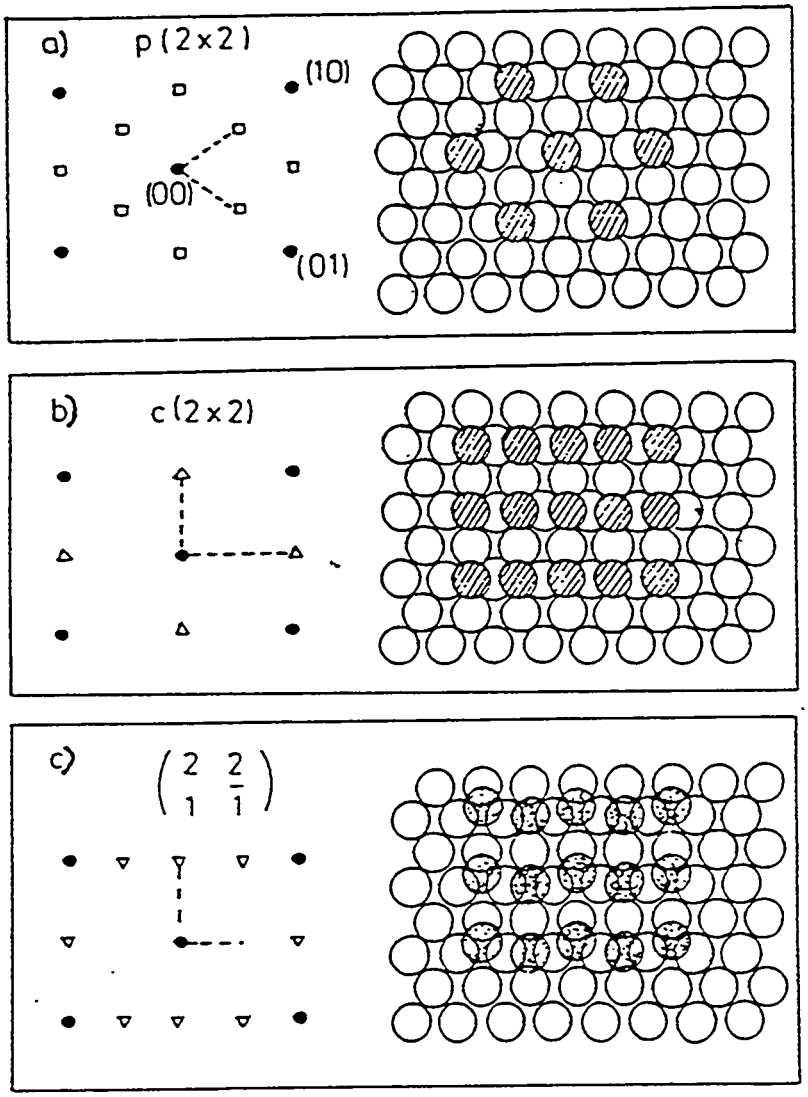

We have been able to reproduce the higher coverage region of this phase diagram, confirming a temperature dependent phase transition from the c(2x2) pattern to the (2 1 -1 1) pattern. Heating a sulfur-saturated surface to 1250K produces an S coverage close to 0.5 ML. On cooling a c(2x2) pattern appears, which changes to the matrix pattern at 500K. Heating the S layer initially to 1350K to lower the S coverage to about 0.4 ML changes the phase transition temperature to about 400K. Presently we are working to reproduce the lower coverage portion of the phase diagram thus establishing a S coverage vs. annealing temperature calibration.

Since our electrochemical sulfur deposition is restricted in area by the diameter of the exit tube (0.35cm) and the Mo(110) crystal is much larger (1.3cm diameter) we have encountered some difficulties with heterogeneous sulfur distributions on the crystal surface. We are in the process of discovering the optimum annealing temperature to promote lateral S diffusion without desorption. It is thought that for S coverages greater than 0.5-0.66 ML, the excess above that coverage desorbs at temperatures above 1325K [6]. Our work has confirmed that above this temperature S desorbs quickly (<1 min) to re-establish a 0.5ML coverage. At 1100K we have noticed a much more gradual decrease in the S coverage. This leads us to believe that surface diffusion is occurring from areas of high S concentration simultaneously with S desorption.

3.3 Structural determination of the Mo(110) p(2x2) surface

An important concern in this work is the nature of the likely adsorption site for furan on the sulfided Mo surfaces. We have routinely used the highly-ordered p(2x2) structure that forms at a coverage of 0.25 ML in many of our experiments. A low-energy electron diffraction (LEED) study of the clean Mo(110) surface indicated that the spacing between the first two Mo layers was contracted by less than 2% of the bulk interlayer spacing of 2.227 Å [1]. However, the detailed

surface crystallography of the p(2x2)-S system has not been investigated.

We have taken a large amount of normal incidence I(V) data for this system and compared it with calculations based on the automated directed search Tensor LEED (TLEED) method [8]. This new perturbative approach to LEED calculations allows for the efficient investigation of many hundreds of possible surface structures involving different adsorption sites and substrate relaxations. In our case we have used the coordinates of the top two Mo layers and the S adatom (plus the inner potential) as independent parameters that are iteratively minimized to produce the best fit between calculations and experiment.

The p(2x2)-S structure was generated by adsorbing a saturation amount of S on a Mo(110) surface from an electrochemical source and then annealing to form the 0.25ML p(2x2)-S structure as described earlier. Images of the fluorescent LEED screen were recorded at 208K using a computer-controlled video camera/image capture board (Oculus 200) over an energy range of 60-220 eV at 4 eV intervals for normal incidence of the electron beam (determined visually by the appearance of LEED beams). These images were stored directly on the hard-disk of the computer. Recording time was less than 15 minutes per dataset. Data were also taken at off-normal incidence but have not been used in this study as the TLEED computer codes at present do not allow off-normal incidence. I(V) curves were then produced by off-line analysis of the stored images using in-house software incorporating novel image-processing transform and object recognition techniques that allow reliable identification, sizing and background substraction of LEED spot intensities without any operator intervention or assumptions about the spot shape [9]

The final experimental dataset consists of 13 non-equivalent beams (equivalent beams were averaged). The labelling of these beams is shown in Figure 3.9.

Figure 3.9. Schematic of the LEED pattern from Mo(110) p(2x2)-S showing beam labelling.

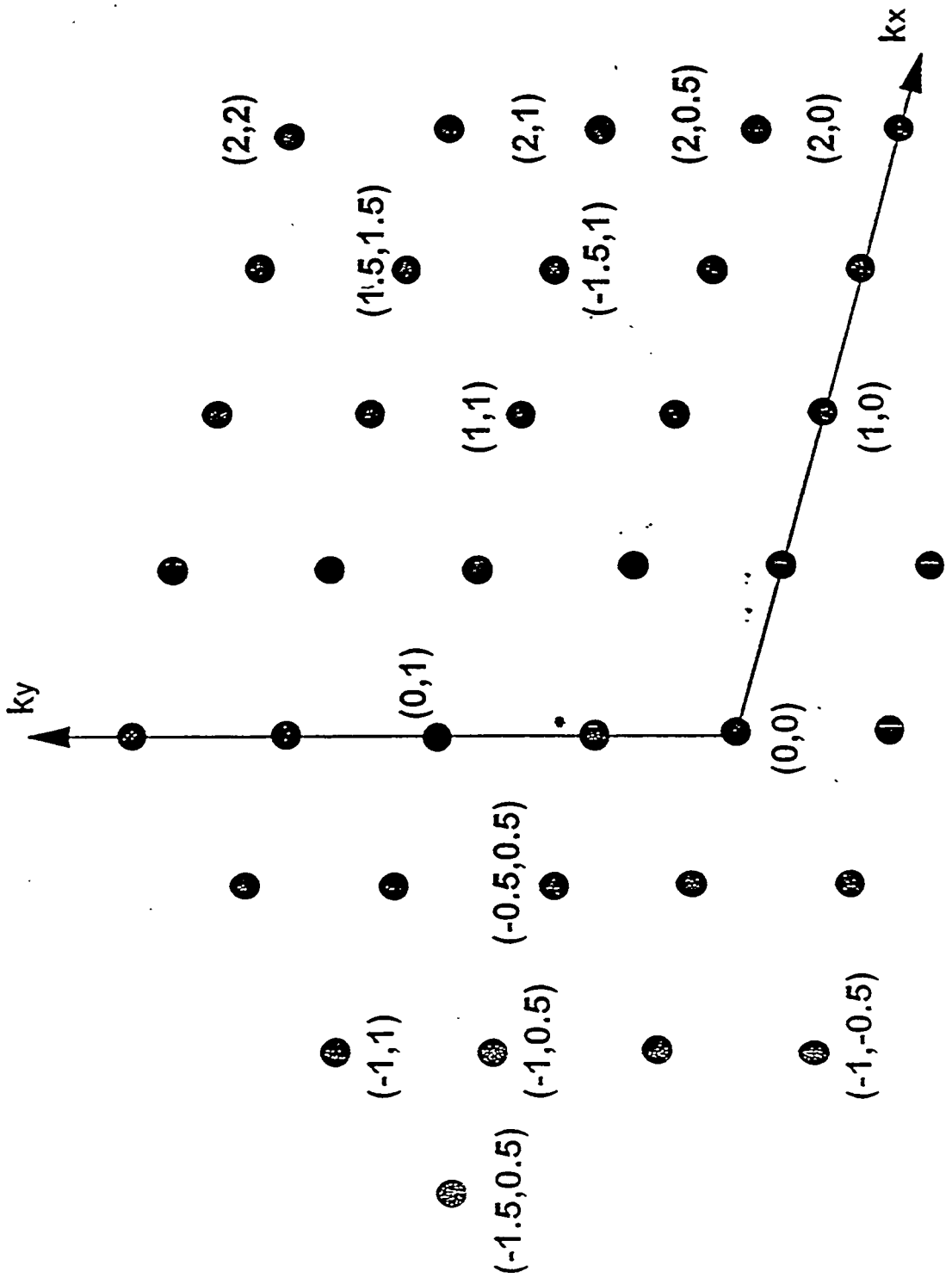

Beams measured: (0,1), (1,1), (-1,1), (2,0), (2,1),(22)

(-0.5,0.5), (-1,0.5), (-1,-0.5),(-1.5,0.5),(1.5,1),(1.5,1.5),(2,0.5)

For the calculations we have used the TLEED package of Van Hove et al [10] on a VAX 9000 computer. These routines automatically adjust the coordinates of surface atoms (and the real part of the inner potential V_{or}) away from the those of a reference structure to find the best fit of calculated I(V) curves with experiment via, in our case, the Pendry R-factor [11] and the Powell direction-set. We used phase shifts up to $l = 7$ taken from the listings found in the conventional Van Hove LEED package while other parameter values were:

θ_D (Mo) = 470 K θ_D(S) = 335 K

V_{or} = 10 eV (initial value) V_{oi} = -4.25 eV

The Mo(110) surface has an oblique unit cell with the symmetry of two mirror planes. The unit cell vectors are separated by an angle of 70.5° (Figure 3.10) with the second Mo layer 2.227 Å distant along the surface normal. The unit cell vectors and the interlayer vector are:

a_x = 2.6876 a_y = 0.4618 Å

b_x = 0.4618 b_y = 2.6876 Å

Interlayer vector: (1.5746, 1.5746, 2.2270) Å

Ignoring on-top adsorption, which experience indicates is unlikely for an adsorbate such as sulfur, there are several obvious high-symmetry adsorption sites on this surface - in the two-fold coordinate bridge sites, in the center hollow (CH) site, which has two atoms in close coordination and two further away, and the three-fold coordinate site (3F). Given the known tendency for relatively large atoms like S to bond in high-symmetry sites, we used the latter two adsorption sites with the S atom 1.5 Å above the first Mo atomic layer as reference structures for the TLEED optimization (these

3.10. Structure of the ideal Mo(110) surface. The surface has an oblique unit cell with the symmetry of 2 mirror planes. The small black circles represent the location of the 3F and CH sites are indicated. The hatched and dark large circles represent first and second layer Mo atoms respectively.

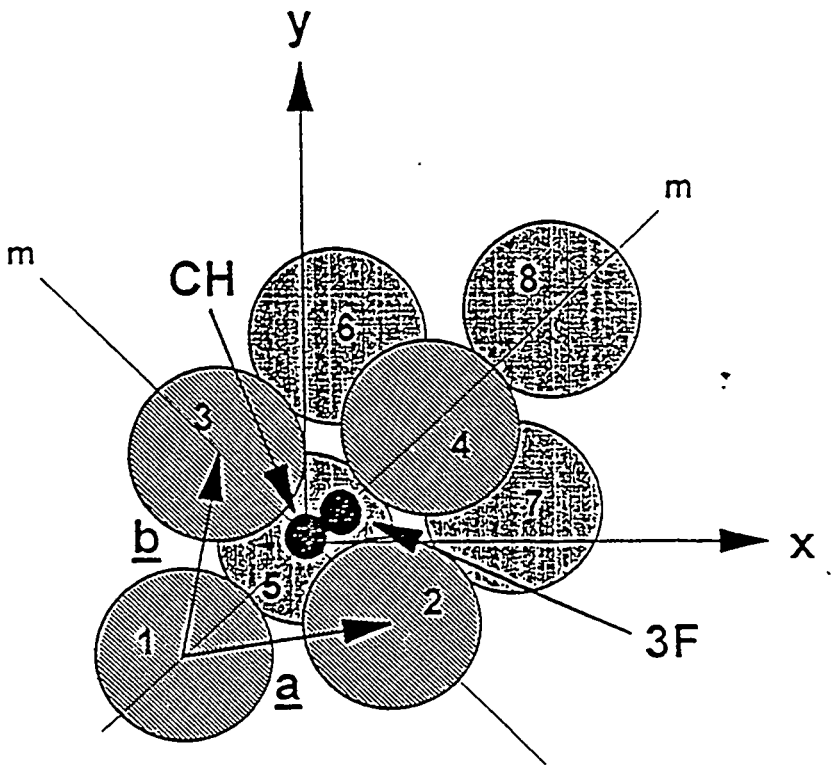

	z (Å)	x (Å)	y (Å)
S adatom 3F site	0.0000	1.0500	1.0500
CH site	0.0000	0.0000	0.0000
Mo layer 1 - Mo1	1.5000	-1.5746	-1.5746
Mo2	1.5000	1.1129	-1.1129
Mo3	1.5000	-1.1129	1.1129
Mo4	1.5000	1.5746	1.5746
Mo layer 2 - Mo5	3.7270	0.0000	0.0000
Mo6	3.7270	0.4618	2.6876
Mo7	3.7270	2.6876	0.4618
Mo8	3.7270	3.1492	3.1492

Table 3.2. Coordinates of atoms comprising 3F and CH adsorption site reference structures

coordinates are listed in Table 3.2). For an undistorted CH site, only one domain is possible, but in the lower symmetry 3F site, and for positions along the mirror plane that link the two sites, averaging of the intensities from the two possible domains is necessary.

We allowed the TLEED program to adjust the coordinates of the S adatom and the 8 Mo atoms that define the first two layers of the substrate. This was accomplished by making one composite layer of the S adatom plus the first layer Mo atoms and a second layer of just the second layer Mo atoms. In this study we restricted the movements of the S and Mo atoms to preserve the symmetry of the mirror plane that links the two high symmetry adsorption sites.

The TLEED routines proceed via iterations in which all the parameters involved (here 16 independent structural parameters and the inner potential) are varied systematically one-by-one to minimize the R-factor. After all the parameters have been optimized in that iteration, if the R-factor has changed by more than 0.005 since the last iteration, then a new iteration begins.

The I(V) curves produced from the CH reference structure calculation were in some cases in better visual agreement with experiment than those from the 3F calculation. For some I(V) curves it proved difficult to judge with any degree of confidence that one calculation was in substantially better agreement than the other. However, running the second part of the TLEED programs quickly showed that the structure derived by starting from the CH adsorption site produced generally better agreement than that derived from the 3F site. Figure 3.11 shows the change in the Pendry R-factor in successive iterations of the TLEED calculation starting from either the 3F or CH reference structure. The 3F site quickly optimizes after 11 iterations to a minimum R-factor of 0.370. The CH site finally optimizes after 20 iterations to a lower Pendry R-factor of 0.298.

Figure 3.12 shows the variation in the parallel components of the best fit S atom location as

3.11. Changes in the Pendry R-factor starting from the 3F and CH reference structures with successive iterations of the TLEED optimization. The iterations cease when the value of the R-factor changes by less than 0.005 and hence the two curves have different extents.

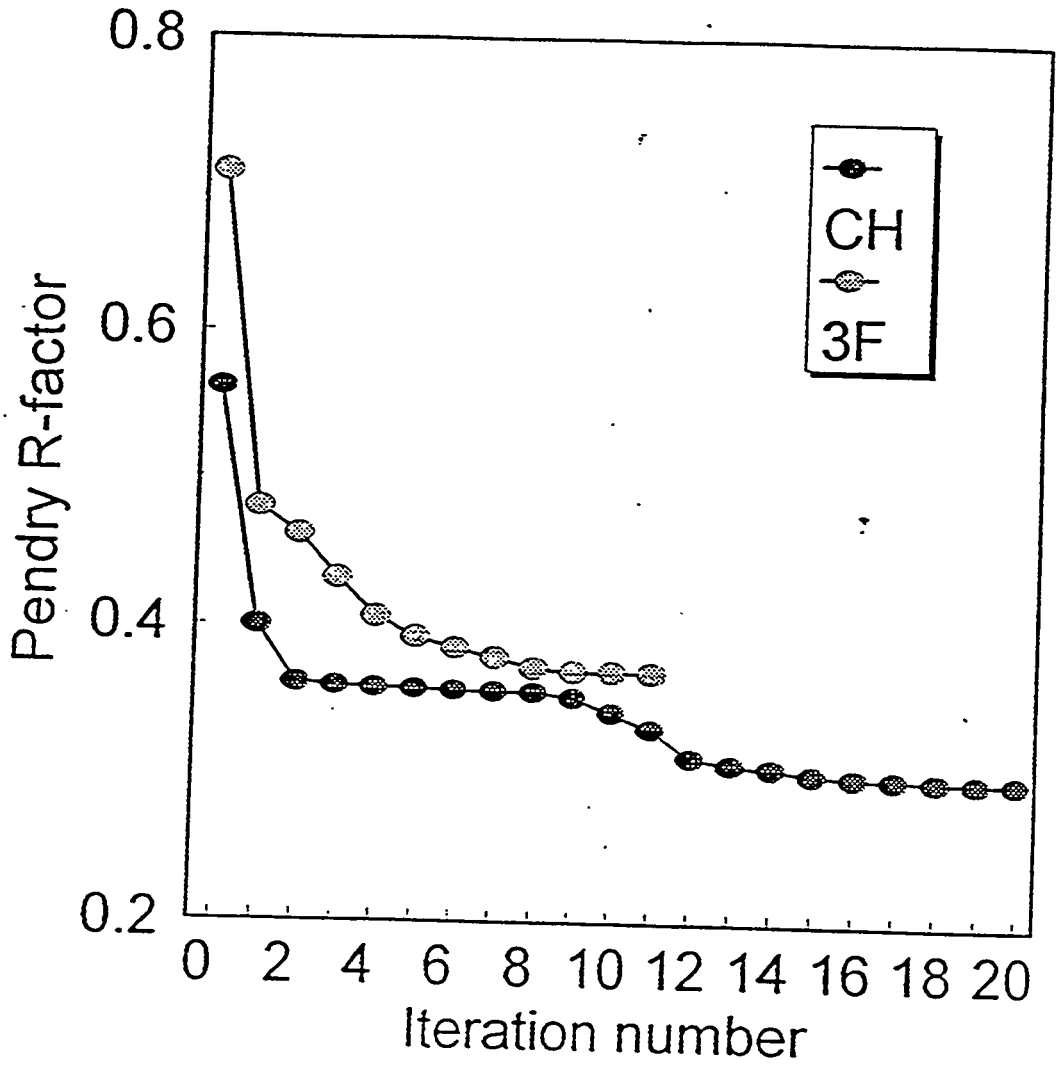

3.12. Changes in the in-plane (x,y) coordinates of the best-fit location of the S atom starting from the 3F and CH reference structures with successive iterations of the TLEED optimization. Delta R(3F-CH) expresses the amount of movement of the S adatom away from the reference structure location along the line that links these two sites. The iterations cease when the value of the R-factor changes by less than 0.005 and hence the two curves have different extents. The value of the Pendry R-factor for the converged optimized structures are given next to each curve.

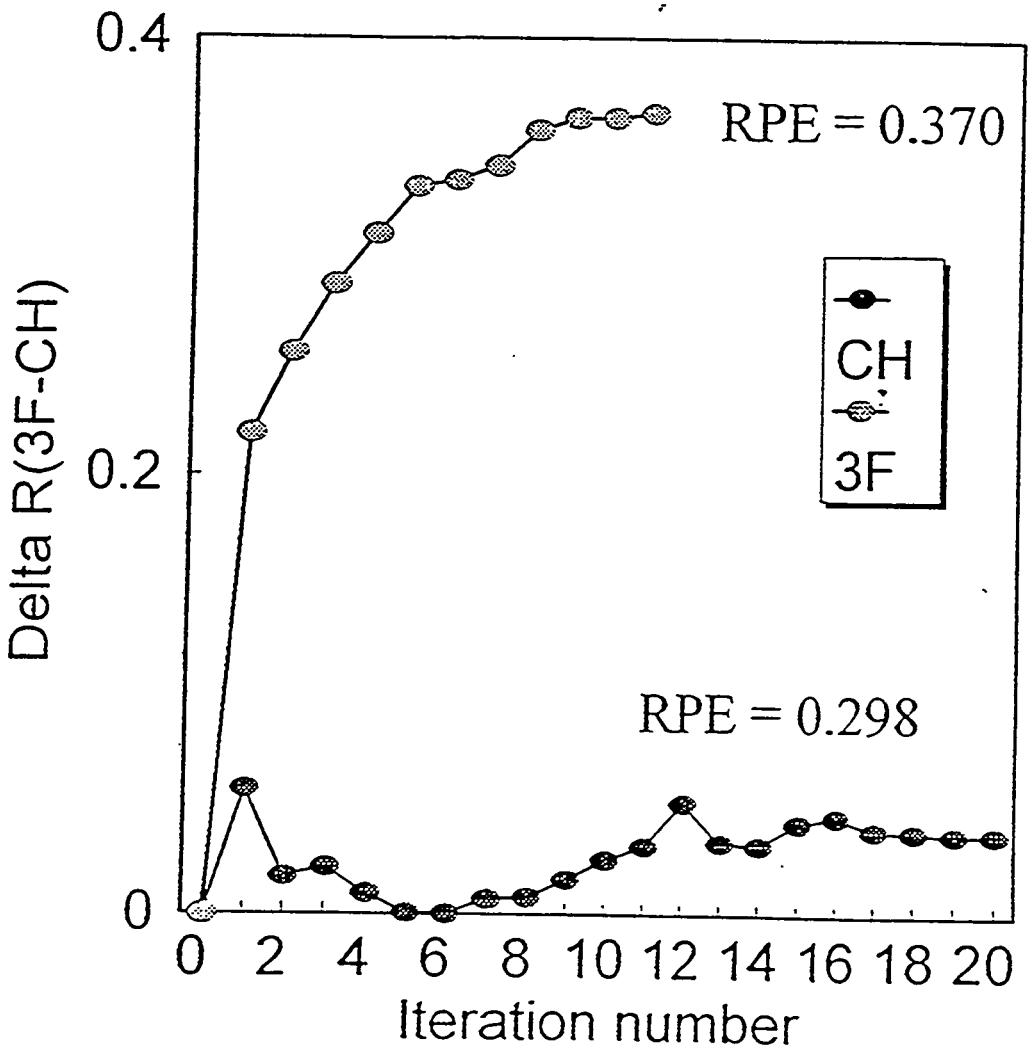

the position of this atom is optimized in successive iterations of the TLEED calculation (the atom is constrained to move along the line between the 3F and CH sites). Starting from the 3F site reference structure the atom always moved in the direction of the CH site; the final converged position of the S atom has it moved over 0.3 Å towards the CH site. Calculations starting from the CH reference structure always resulted in an optimized structure with in-plane coordinates for the S atom that were within 0.025 Å of the S atom location in the reference structure. Allowing the optimization to start from different S adatom starting positions along the line linking the CH and 3F sites produced the same result, indicating that this optimized structure derived from the CH site probably represents a global rather than a local minimum. The representative IV curves for one integral beam and one half-order beam shown in Figure 3.13 lead to us to conclude that the optimized structure is close to the true one. The remaining discrepancies may be due to some problem in the experiment, such as the angle of incidence being set incorrectly, or may indicate that the present structure needs refinement.

The coordinates of the 9 atoms that make up this optimized Mo(110) p(2x2)-S structure are collected in Table 3.3 and the structure is displayed in Figures 3.14 and 3.15. The S atom lies close to the CH location set in the reference structure, shifted slightly (by 0.03 Å) along the cell diagonal. However, the Mo2 and Mo3 atoms that were closest to the S atom in the reference CH structure move outward (in the x and y directions respectively) by about 0.3 Å, while Mo4 moves along the cell diagonal an equivalent amount to the movement of the S atom. Also the first Mo layer is rumpled with Mo2 and Mo3 depressed by 0.08 - 0.14 Å relative to Mo1 and Mo4, while the second Mo layer shows less vertical rumpling. The most significant lateral movement in the second Mo layer is that of Mo5 that moves along the unit cell diagonal by close to 0.2 Å.

3.13. IV curves from the (-1,1) and (-1,-1/2) beams from Mo(110) p(2x2)-S. The solid line is the results of the TLEED calculation and the lines with points are the experimental data.

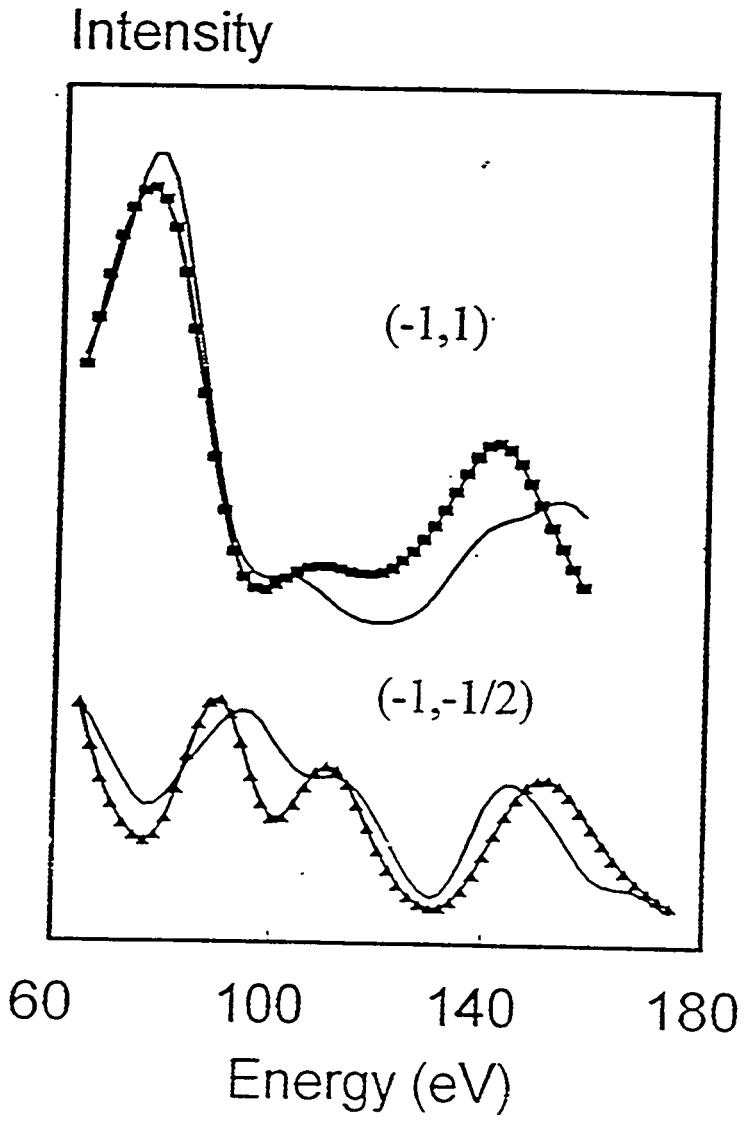

Atom	z (Å)	Δz (Å)	x (Å)	Δx (Å)	y (Å)	Δy (Å)
S	-0.00	-0.00	0.03	0.03	0.03	0.03
Mo1	1.626	0.13	-1.57	0.01	-1.57	0.01
Mo2	1.705	0.21	1.42	0.31	-1.14	-0.03
Mo3	1.705	0.21	-1.14	-0.03	1.42	0.31
Mo4	1.571	0.07	1.60	0.03	1.60	0.03
Mo5	3.770	0.04	0.15	0.15	0.15	0.15
Mo6	3.780	0.05	0.56	0.10	2.66	-0.03
Mo7	3.780	0.05	2.66	-0.03	0.56	0.10
Mo8	3.814	0.09	3.11	-0.04	3.11	-0.04

Table 3.3. Coordinates of atoms and the shifts from the coordinates of the CH reference structure of Table 3.2 for the optimized Mo(110) p(2x2)-S structure. These values vary by as much as ± 0.05 Å if the calculations start from different initial positions along the line joining the CH and 3F sites. We did not investigate the effect of changing the non-structural parameters such as inelastic damping and Debye-Waller effects. The optimized inner-potential value is 8.03 eV.

3.14. The TLEED optimized Mo(110) p(2x2) - S structure. The hatched and dark large circles represent first and second layer Mo atoms respectively. The S adatoms are shown as black circles with diameters smaller than the atomic radius for clarity. Arrowheads show the direction of movement of substrate atoms relative to their locations in the bulk structure shown in Figure 2.

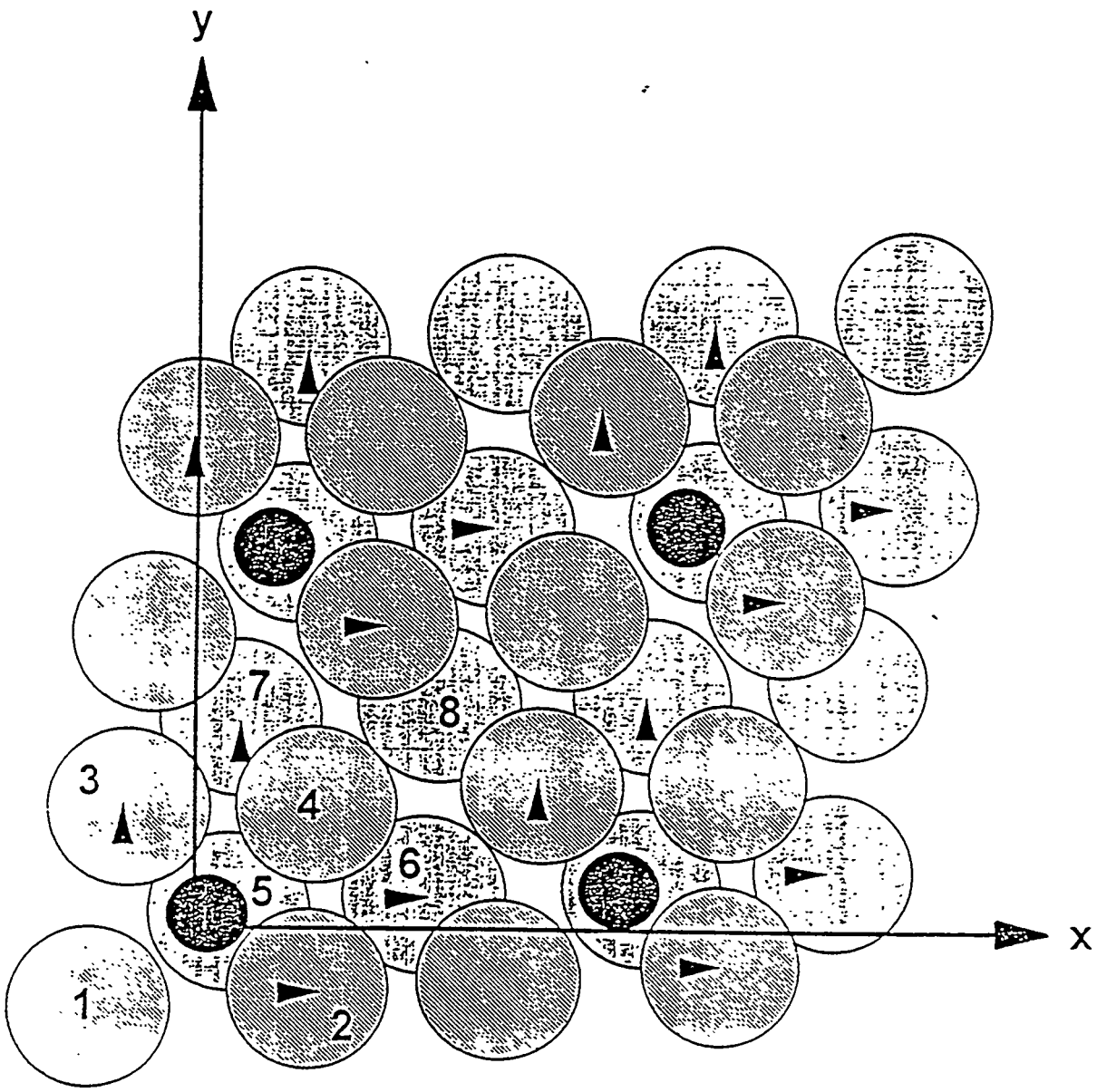

3.15 A cross-section through the TLEED optimized Mo(110) p(2x2) - S structure of Figure 3.13 along the direction linking Mo1 and Mo4. Atoms with dashed outlines lie off this line and are projected onto it. The numbers indicate vertical shifts of atoms in Å from their bulk locations (shown as the long solid lines) e.g. Mo4 has moved down from its bulk location by 0.07 Å

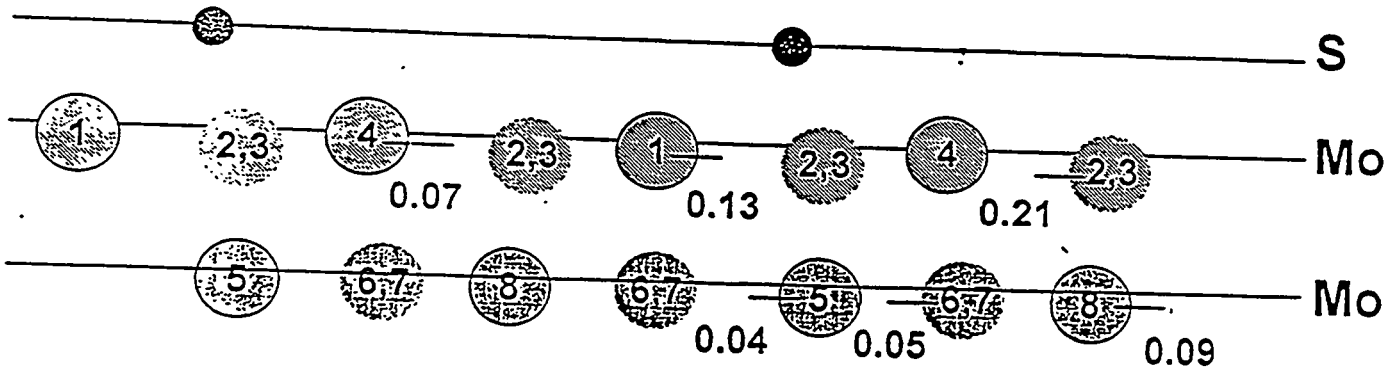

The end result of these substrate shifts is that the S adatom is located in a distorted central hollow. This distortion is such that the final coordination of the S atom is rather closer to 3-fold coordinate rather than the 2+2 coordination characteristic of the undistorted CH site. There are now three slightly different Mo-S bond lengths:

Mo1 - S : 2.78 Å

Mo2,3 - S : 2.49 Å

Mo4 - S : 2.72 Å

The shortest bond-length between Mo2,3 and the S atom is less than the sum of atomic (hard-sphere) radii of 2.65 Å. Mo1 lies slightly deeper than Mo4 and therefore has the longest bond length.

Shih et al [12] have studied the structure of the analogous Fe(110) p(2x2)-S system by a conventional LEED method. Their results placed the S adatom in the middle center hollow site surrounded by 4 Fe atoms that are laterally shifted in a different manner to that which we have found for Mo. In their structure the Fe atoms remain in the same relative locations to one another as in the bulk, but the unit cell of the top layer is contracted symmetrically with respect to the bulk unit cell. The overall effect is that the Fe atoms are "attracted" to the adatom, leaving more open areas between the S-Fe_4 units. We should note they to some extent selected for this structure by only examining structures that preserved the rectangular symmetry of the surface unit cell. In addition they did not allow for surface rumpling of the sort we find for the Mo system.

3.4 References

1. L.J. Clarke, Surface Sci. 102 331 (1981).

2. M. Salmeron, G.A. Somorjai and R.R. Chianelli, Surface Sci. 127 526 (1983).

3. M.H. Farias, A.J. Gellman, G.A. Somorjai, R.R. Chianelli and K.S. Liang, Surface. Sci. 140

181 (1984).

4. V. Maurice, L. Peralta, Y, Berthier and J. Oudar, Surface Sci. 148 623 (1984).

5. L. Peralta, Y. Berthier and J. Oudar, Surf. Sci. **55**, 199 (1976).

6. A. Sanchez, J.J. De Miguel, E. Martinez and R. Miranda, Surf. Sci. **171**, 157 (1986).

7. W. Witt and E. Bauer, Ber. Bunsenges. Phys. Chem. **90**, 248 (1986).

8. P.J. Rous, M.A. Van Hove and G.A. Somorjai, Surf. Sci. **226**, 15 (1990).

9. J. Toofan and P.R. Watson, J. Vac. Sci. Technol. A in press

10. M.A. Van Hove, P.J. Rous, A. Wander and A. Barbieri, Lawrence Berkeley Laboratory, Berkeley, CA 94720 (kindly supplied by Dr. Van Hove).

11. J.B. Pendry, J. Phys. C: Solid State Phys. **13**, 937 (1980)

12. H.D. Shih, F. Jona, D.W Jepsen and P.M. Marcus, Phys. Rev. Lett. **46**, 731 (1981).

4. Adsorption of hydrogen

4.1 H(D) adsorption on clean Mo surfaces

Figure 4.1 shows a series of deuterium thermal desorption spectroscopy (TDS) traces after various exposures of Mo(110) to deuterium. Deuterium is used rather than hydrogen itself as the TDS signal is much cleaner than that from hydrogen because of the very low background at AMU 4 compared to AMU 2; experience with other systems has shown that deuterium TDS is almost identical to hydrogen TDS and we shall refer to deuterium and hydrogen interchangeably. Our data is very similar to that of Mahnig and Schmidt [1] if we allow for the slower heating rate in our case. Above 10L exposure to hydrogen the amount of material that desorbs, as measured by the area under

Figure 4.1 Deuterium TDS spectra for various exposures on clean Mo(110).

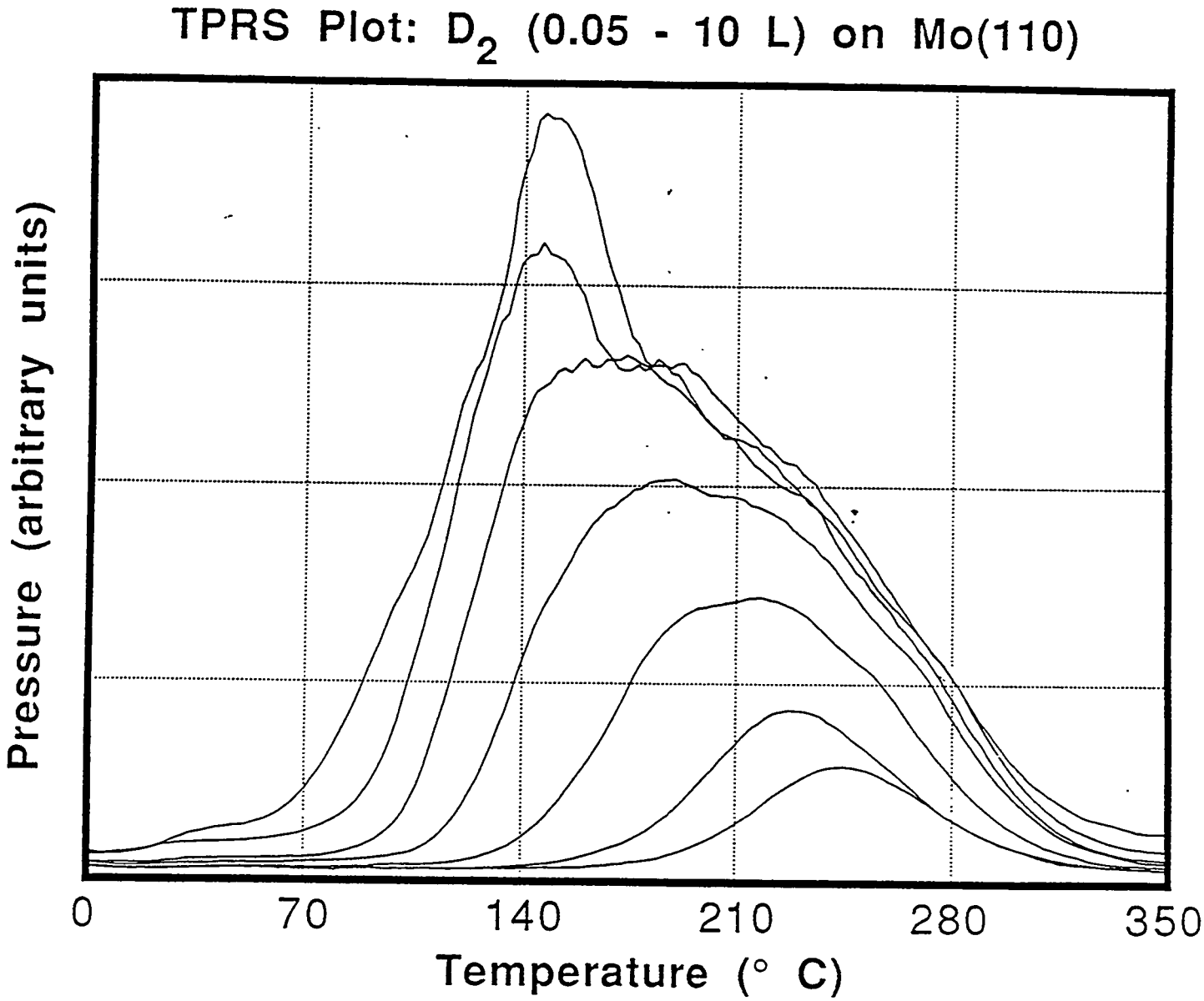

the TDS curve, does not change indicating that the surface has saturated. The saturation coverage hydrogen cannot be directly measured from these experiments, but we can estimate it in the following manner. Zaera et al [2] have shown that on Mo(100) the saturation coverage of hydrogen corresponds to 2 H/Mo. Mahnig and Schmidt [1] found that the maximum hydrogen TDS yield from Mo(110) was just 1/2 of that from Mo(100), indicating a saturation coverage of 1 H/Mo. Given the close agreement between our data and that of Mahnig and Schmidt, we therefore will assume that the saturation coverage that occurs at about 10L exposure corresponds to a hydrogen coverage equal to 1.0 ML. With this assumption we can construct an uptake curve for hydrogen on the clean Mo(110) surface as shown in Figure 4.2.

The D_2 TDS curves shown in Figure 4.1 can be interpreted in the following manner. At the lowest hydrogen coverages, hydrogen desorbs in a single symmetric peak (designated β_2 by Mahnig and Schmidt) centered at about 230°C. As the hydrogen coverage is increased this peak increases in area and shifts to lower temperature. At about 1L exposure this peak saturates and a second β_1 peak appears at about 165°C that also shifts to lower temperature with increasing hydrogen coverage. The behavior of these peaks are indicative of second-order desorption processes. In the case of the low-coverage data, where we can easily isolate the β_2 peak, we can analyze the data to extract the kinetic parameters. The simplest approach is that of Redhead [3], who showed that if the energy of desorption (E_d) and the frequency factor (ν) are independent of the hydrogen coverage (Θ_H), then the peak maximum (T_m) is related to the coverage by:

$$\ln(T^2_m \Theta_H) = (E_d/R)(1/T_m) + \ln(\beta E_d/R\nu)$$

Figure 4.2 Uptake of deuterium on clean Mo(110)

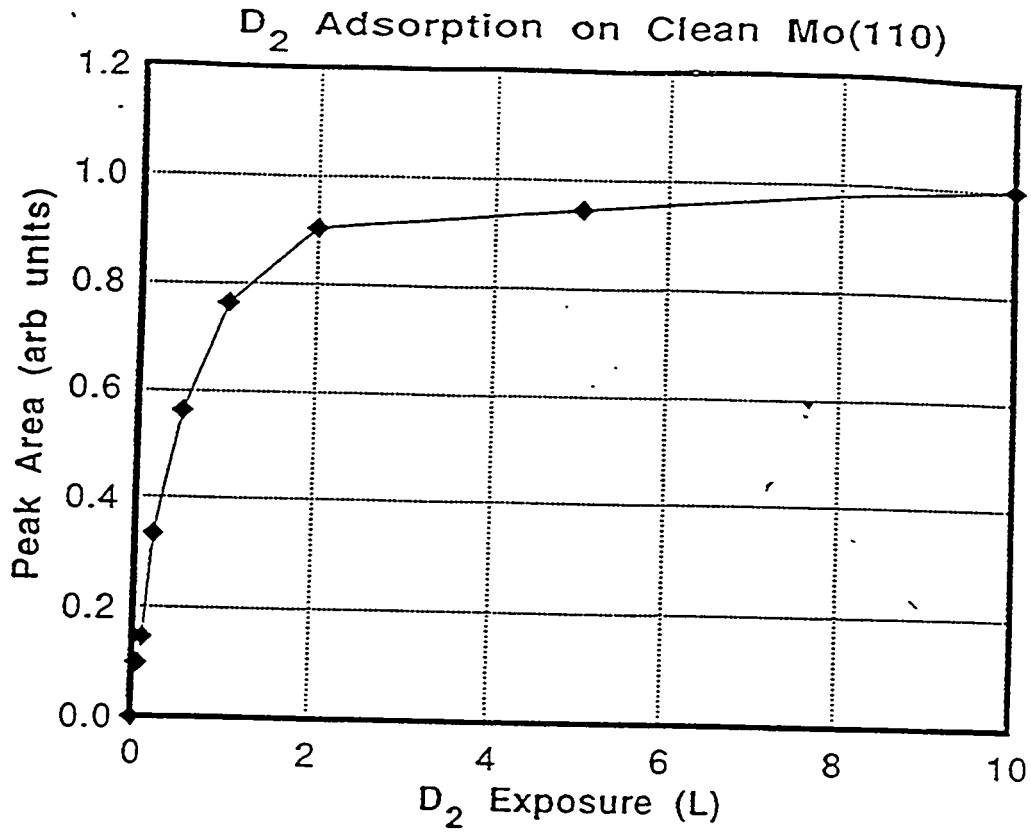

Figure 4.3 2nd-order Redhead plot for the low-coverage data of Figure 4.2

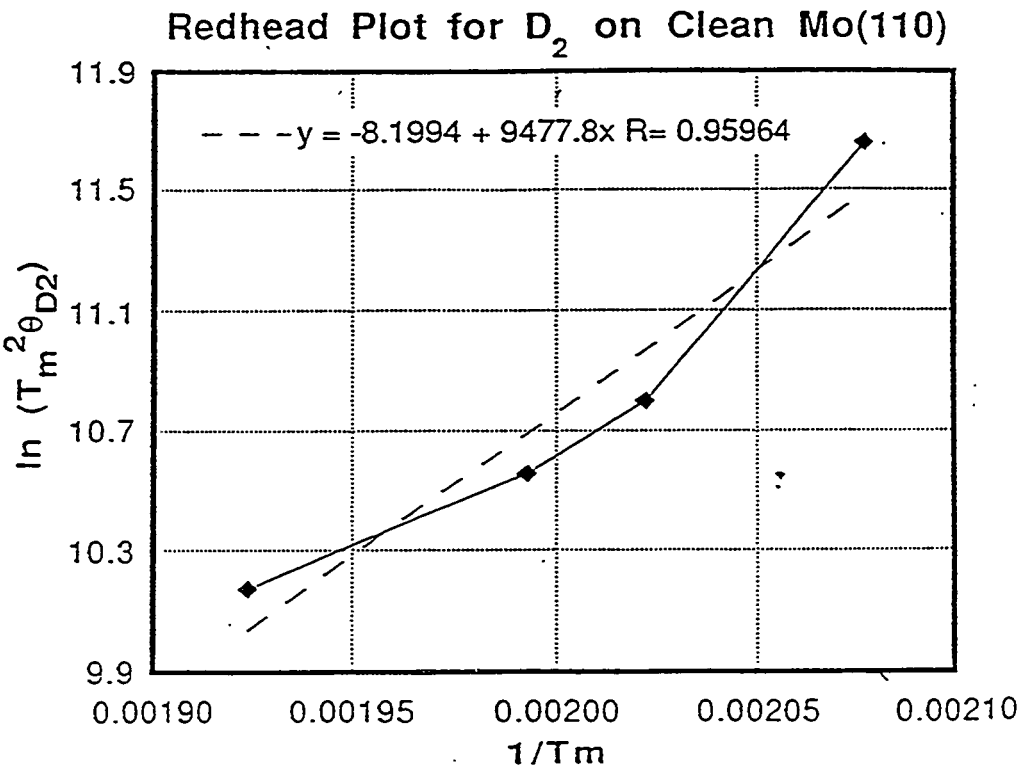

This relationship is plotted in Figure 4.3 and yields a value of E_d = 19 kcal/mol. The curve is not a true straight line because of the assumption of no changes in the kinetic parameters with coverage. More complex procedures are available [4] to more accurately evaluate these parameters.

The origin of the high-coverage peak is not clear. It could result from occupation of a second type of adsorption site, but King [4] has argued for the H/W(110) system that the occurrence of two peaks at high hydrogen coverages is due to interactions among the adsorbate atoms that become important as the surface concentration of hydrogen increases.

4.2 H(D) adsorption on sulfided Mo surfaces

Preadsorption of sulfur on the Mo(110) surface has a dramatic effect on the amount of hydrogen that can be adsorbed, and on the position of the hydrogen TDS peaks. Figure 4.4 contrasts the TDS signals from the clean Mo(110) surface with that from a surface with 0.4 ML of sulfur on the surface. We can see that the amount of hydrogen adsorbed is greatly reduced, at about 0.5 ML of sulfur no hydrogen can be adsorbed - that is the surface is completely blocked towards hydrogen adsorption. The hydrogen that does desorb does so with similar peak shapes to that from the clean surface, but at much lower temperatures. The severity of these effects scales with the sulfur coverage as is demonstrated in Figure 4.5. Here the saturation coverage and peak maximum can be seen to move to lower values as the amount of sulfur on the surface increases.

The fact that the hydrogen TDS peak temperatures are shifted to lower temperatures relative to the clean surface indicates that the bond between the surface and adsorbed hydrogen is less strong when adsorbed sulfur is present. Thus, if desorption of hydrogen were to be the rate-limiting step during a dehydrogenation process involving hydrocarbon moieties on the surface, then the sulfided surface would allow the reaction to proceed more easily than the clean surface.

Figure 4.4 Deuterium TDS from clean and sulfided Mo(110)

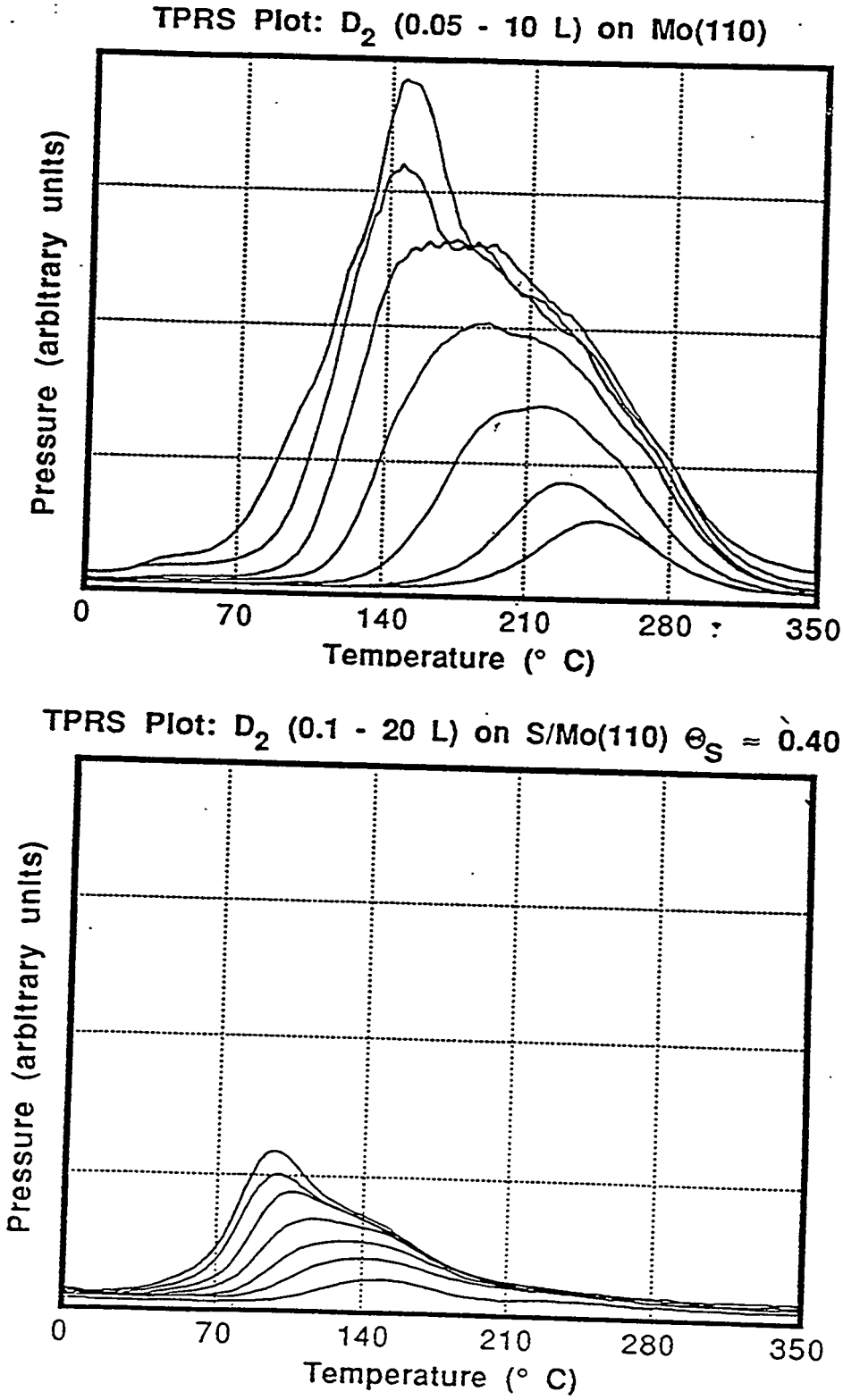

Figure 4.5 Deuterium TDS data for various S coverages on Mo(110)

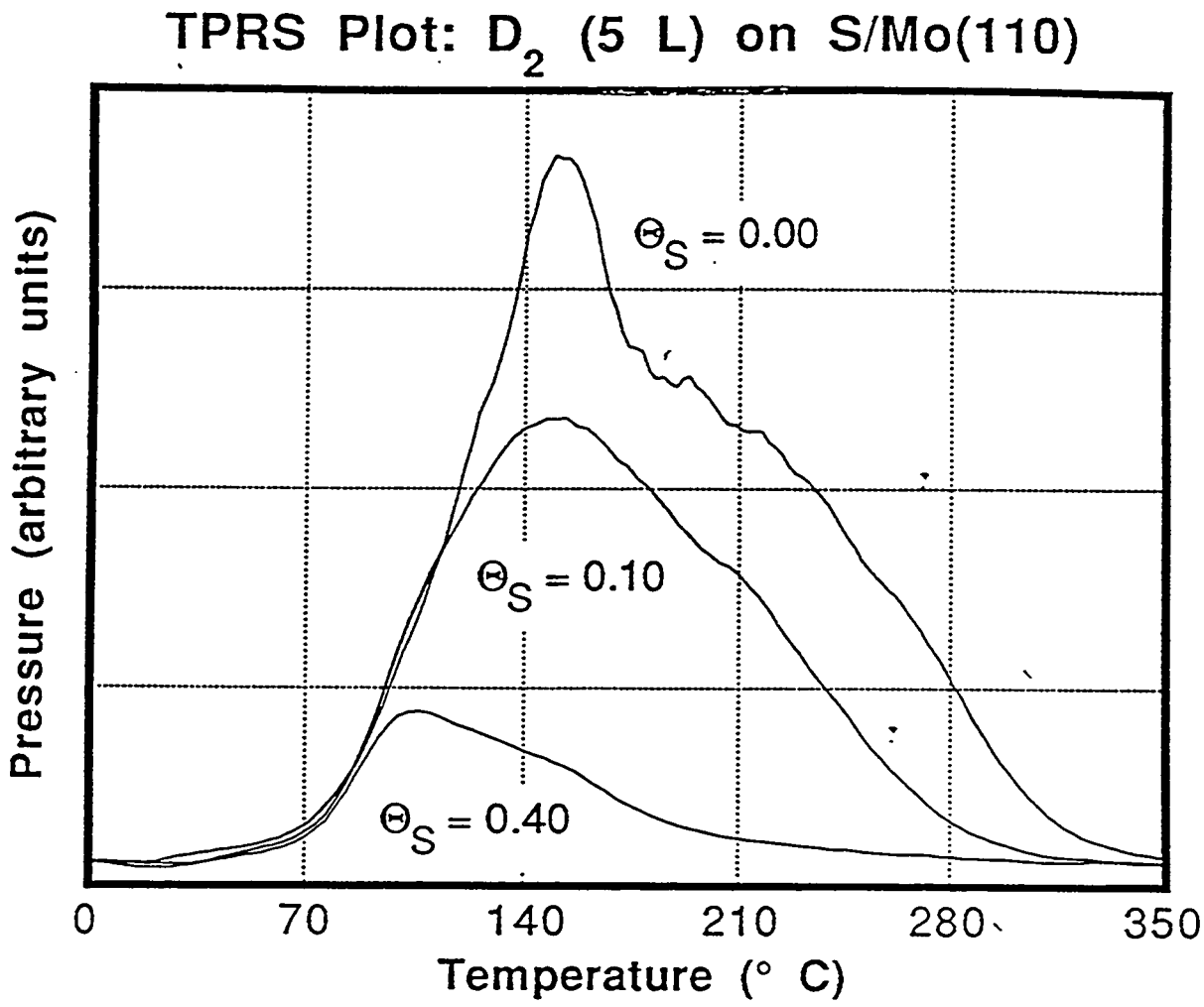

The range of the blocking effect of sulfur on hydrogen adsorption can be investigated in the following manner. If we accept that the desorption is second-order, then the area under a TDS trace should follow a modified Langmuirian form of the type:

$$\text{Area} = (1 - n\Theta_S)^2$$

where Θ_S is the surface coverage of sulfur atoms that block the adsorption of n H_2 molecules each. Figure 4.6 shows the fit of some of the TDS data (for a 5L deuterium exposure) for various assumed values of n. Our experimental data does not seem to follow the expected smooth curves, having something of a stepped appearance, but does seem to fit best for n = 1-1.5. Examination of similar plots for other exposures shows that the apparent stepped appearance of the data is found in all cases and we are pursuing the possible origin of this feature.

It interesting to speculate about the adsorption processes at work here. It is likely by analogy with other systems, but not yet proven, that sulfur adsorbs either in the pseudo-fourfold hollow (4F) sites (A in Figure 4.7), or the 3-fold (3F) sites (B in Figure 4.7) on the Mo(110) surface. It is also most probable by analogy that the hydrogen atoms adsorb on the bridge sites on this surface. The site where the hydrogen molecule dissociates is probably the 3F site, from where the two H atoms can easily move to two nearby bridge sites. Now, if a sulfur atom were already present in the site where a hydrogen molecule would normally dissociate then clearly that molecule would be blocked from adsorption. If we further allow for the size of the adatom then it is possible for one adatom to block more than one such adsorption site. Thus, for instance an S atom adsorbed in the 4F site could block two 3F sites and all four potential H atom bridge sites (Figure 4.7 site A). On the other hand, a sulfur atom adsorbed in the 3F site would still leave some access to the other 3F site (Figure 4.7

Figure 4.6 Fit of deuterium TDS data for sulfided Mo(110).

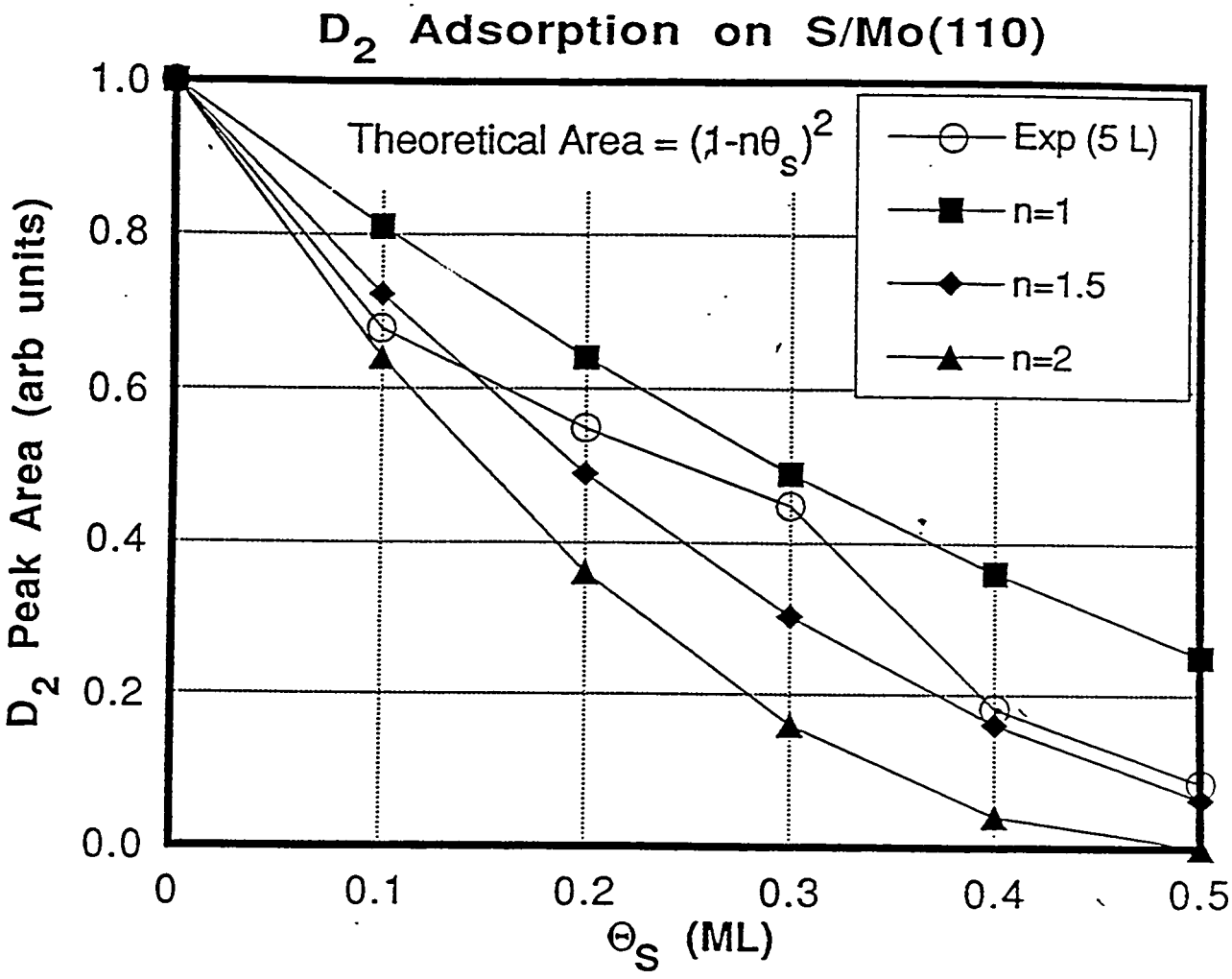

Figure 4.7. Possible adsorption sites for S and H on Mo(110).

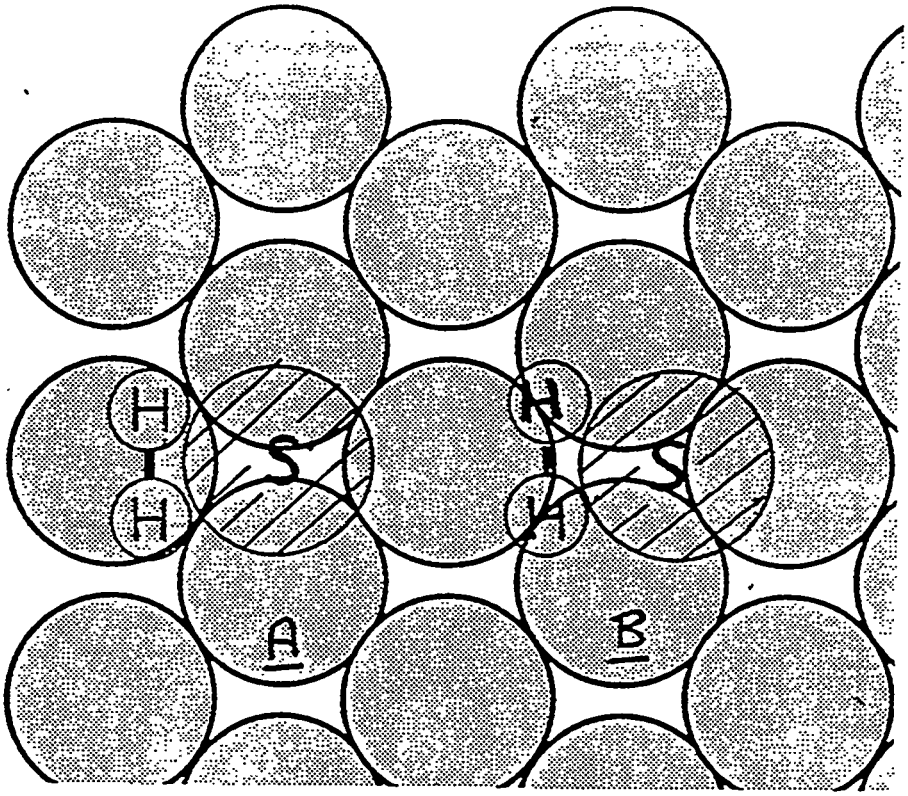

site B) and would leave at least two bridge sites open. The present data tends to support the latter possibility more than the former, but further analysis is needed to clarify this issue.

4.3 H(D) adsorption on carbided Mo surfaces

The preadsorption of carbon on the Mo(110) surface also blocks the adsorption of hydrogen as can be seen in Figure 4.8, where a carbided surface is compared with the clean surface. At this time we do not a good calibration for the surface carbon coverage, but experiments to determine this are underway. As Figure 4.9 shows, the preadsorption of carbon results in a lowering of both peak area and temperatures. The shifts in temperature maximum with are less dramatic than we saw for sulfur preadsorption.

4.4. References

1. M. Mahnig and L.D. Schmidt, Z. fur Physik. Chem. NF 80,71 (1972).
2. F. Zaera, E.B. Kollin and J.L. Gland, Surf. Sci. 166, L149 (1986).
3. P.A. Redhead, Vacuum 12, 203 (1962).
4. D.A. King, Surf. Sci. 47, 382 (1975).

Figure 4.8 Contrasts in deuterium TDS from clean and carbided Mo(110).

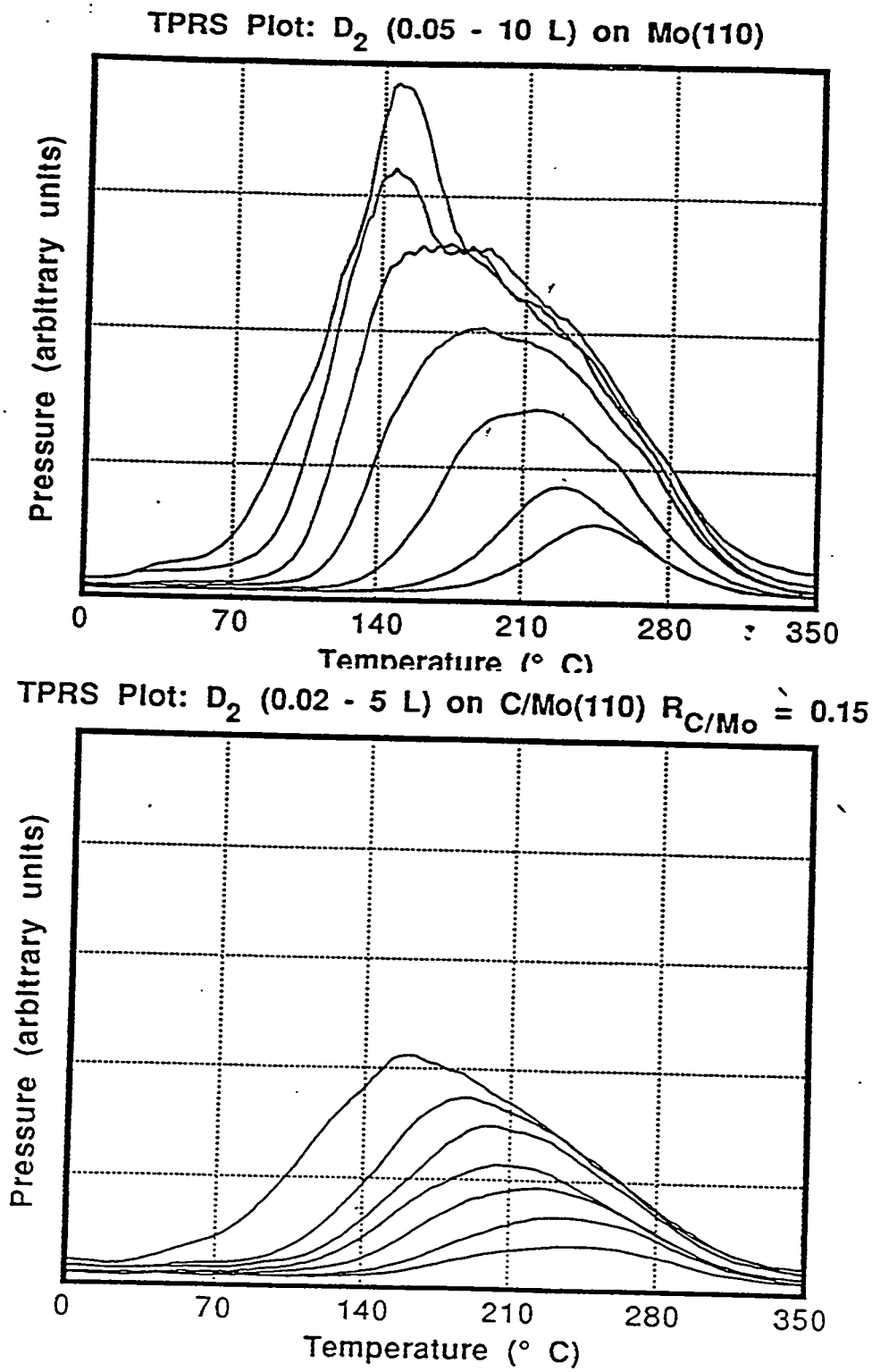

Figure 4.9 Changes in deuterium TDS spectra from carbided Mo(110) surfaces.

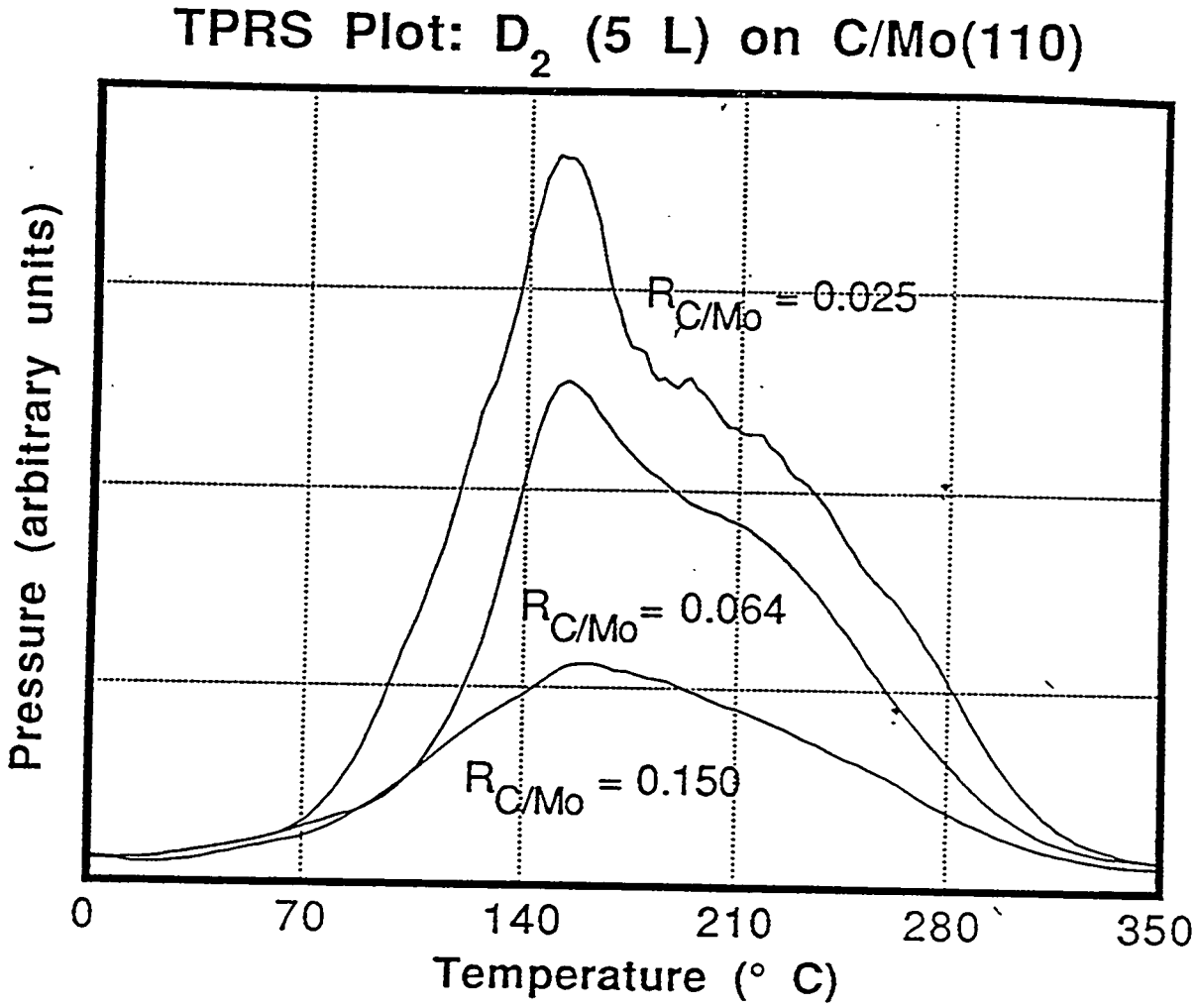

5.1 Furan adsorption on sulfided Mo surfaces

To perform these experiments we must know the form of the mass spectrum of furan measured by the quadrupole mass spectrometer in order to distinguish reaction products from cracking products formed in the ionizer. Figure 5.1 shows such a mass spectrum taken in our apparatus and Table 5.1 list the relative peak intensities. The parent peak occurs at 69 AMU, but the principle peak is at 39 AMU corresponding to C_3H_3, together with C_3H_2 (38 AMU) and C_3H (37 AMU). The other half of the cracked furan molecule appears at 29 AMU (HCO) and 28 AMU (CO), although the latter peak contains a contribution from N_2 due to a small amount of residual air in the furan line.

Table 5.1 Principal peaks in the mass spectrum of furan.

m/e AMU	Intensity
14	14
29	25
37	15
38	16
39	100
40	15
42	14
68	30

Figure 5.1. Mass spectrum of furan.

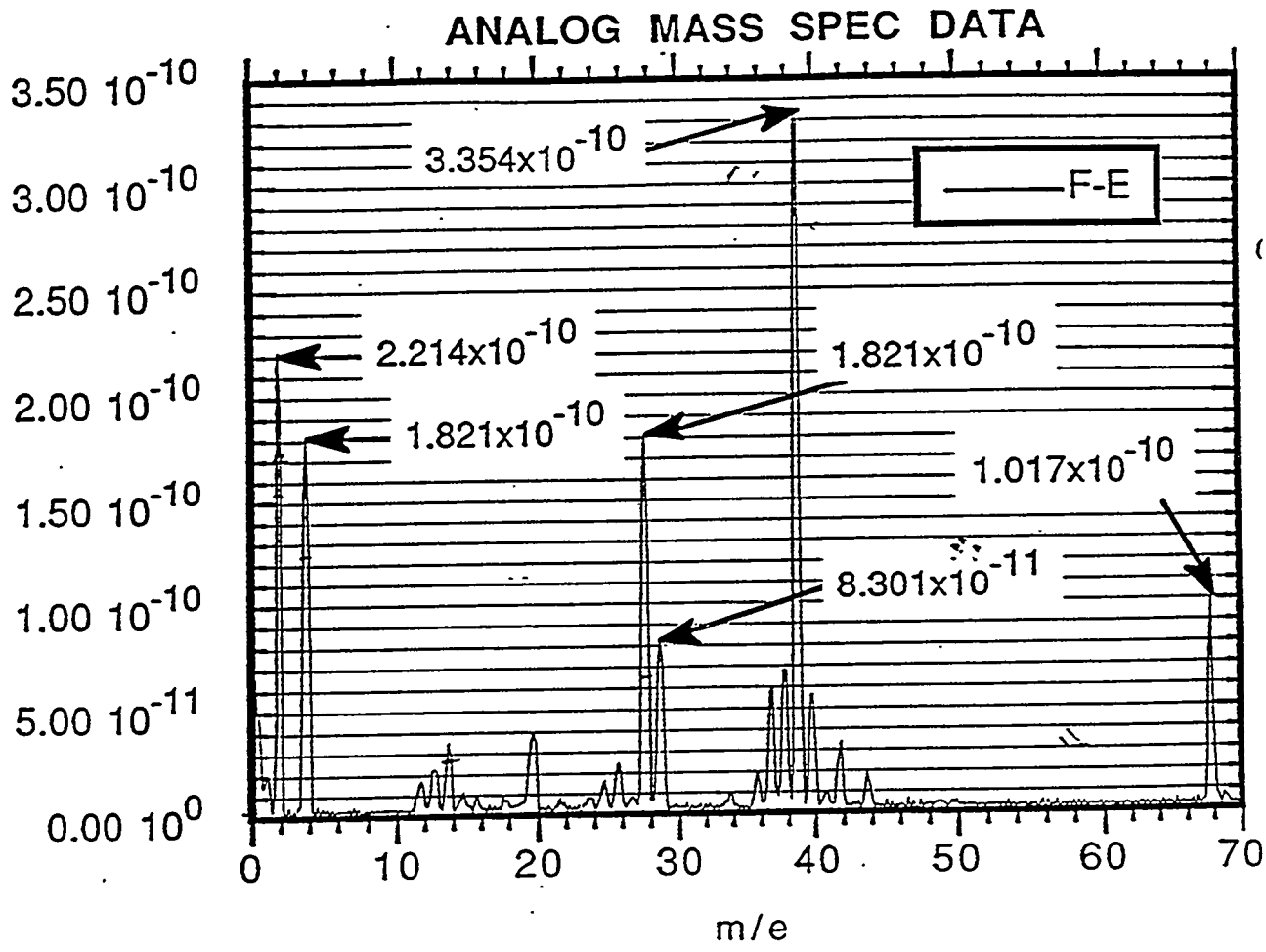

Figure 5.2 shows an example of temperature programmed reaction spectroscopy (TPRS) scans for 2L ($2x10^{-6}$ torr-s) exposure of furan at -50°C to a Mo(100) surface that is covered with 50% sulfur. A small desorption peak due to molecular furan (39 AMU) occurs close to room temperature, but the spectra are dominated by a hydrogen and a 28 AMU signal. The hydrogen signal bears a distinct resemblance to those reported for thiophene TPRS on sulfided Mo [1-3]. The 28 AMU signal is very interesting as it could originate from a number of sources - CO, N_2, C_2H_2 or as cracking from CO_2. We have performed a number of careful checks that indicated that this signal is in fact originating from CO resulting from reaction of furan:

a) if the 28 AMU signal were due to ethylene, then we would expect a substantial (65%) 27 AMU peak. The 27 AMU response is within the noise.

b) if this signal came from dinitrogen, then we would expect a 14 AMU peak at 7% of the 28 AMU intensity - this is not found.

c) we do not observe a 44 AMU peak characteristic of CO_2.

d) if the signal came from CO we expect 12 AMU (5%) and 16 AMU (1%) cracking products. The 16 AMU signal would be too small to observe, but the 12 AMU signal exactly parallels the 28 AMU signal.

e) when no furan is adsorbed, there is no 28 AMU signal.

Hence, it appears that we are generating CO on the surface from furan, and that CO production occurs at several temperatures (Table 5.2). The high temperature CO peaks are observed when CO is adsorbed on a clean or sulfided Mo surface, and is generally attributed to recombination of C and O atoms. The lowest CO peak is close to those observed for molecular desorption, but the peaks between 500-700K are quite unusual.

Figure 5.2 TPRS scan for 2L furan on a Mo(100) surface covered with ~ 0.5 ML sulfur.

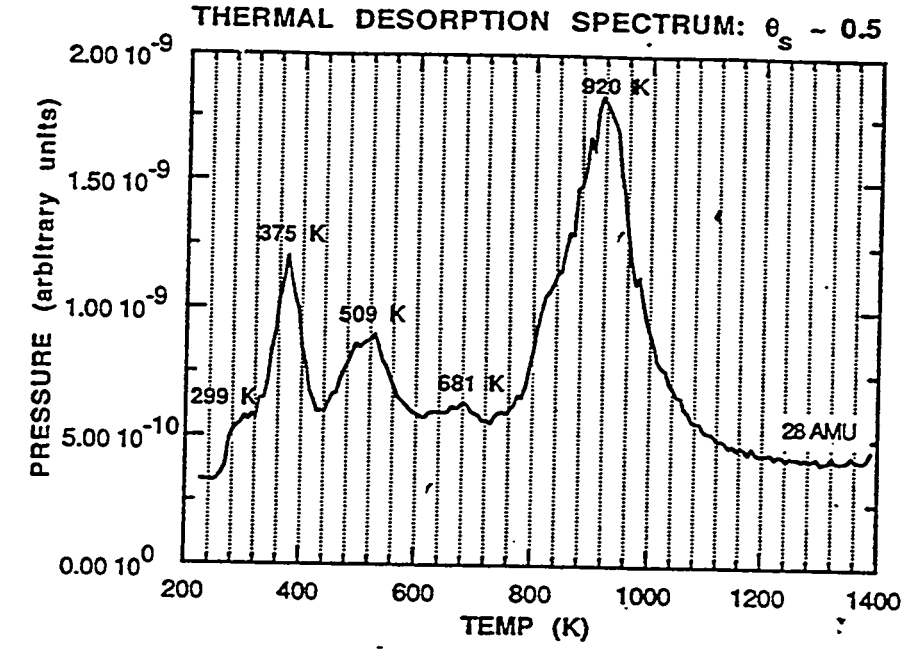

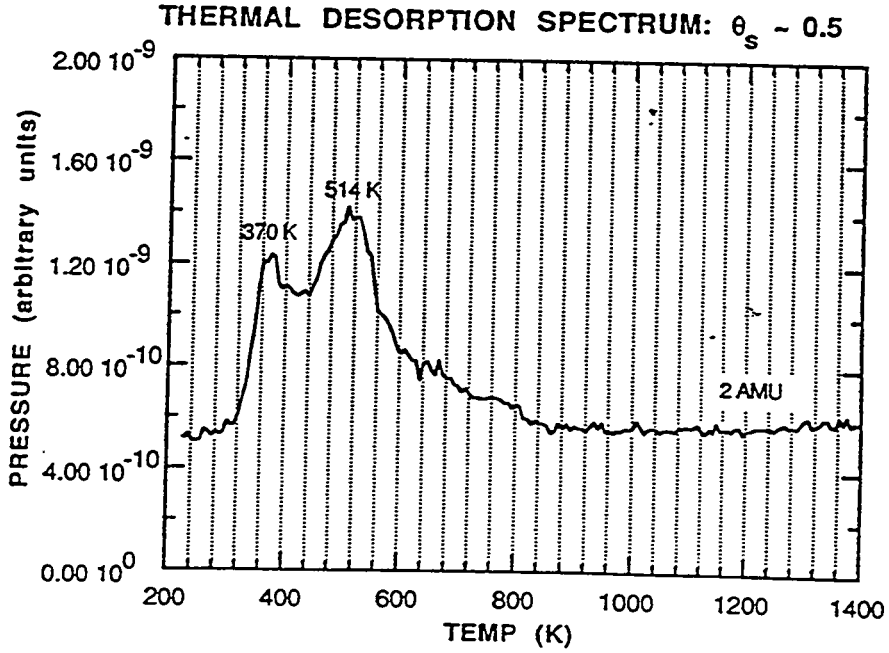

Table 5.2 Desorption temperatures for H_2 and CO on Mo after furan adsorption on sulfided Mo(100).

Adsorbate/ substrate	Mass (AMU)	Desorption temp (K)	Ref.
Furan/Mo-S 0.5ML	2	380 480 660	This work
	28	340 520 680 ??? ???	
CO/Mo-S 0.5ML	28	360 820 950	2
CO/Mo	28	475 1000 1275	3

Figure 5.3 TPRS spectra from a saturation dose (0.5L) furan on Mo(100) with about 0.2 ML sulfur.

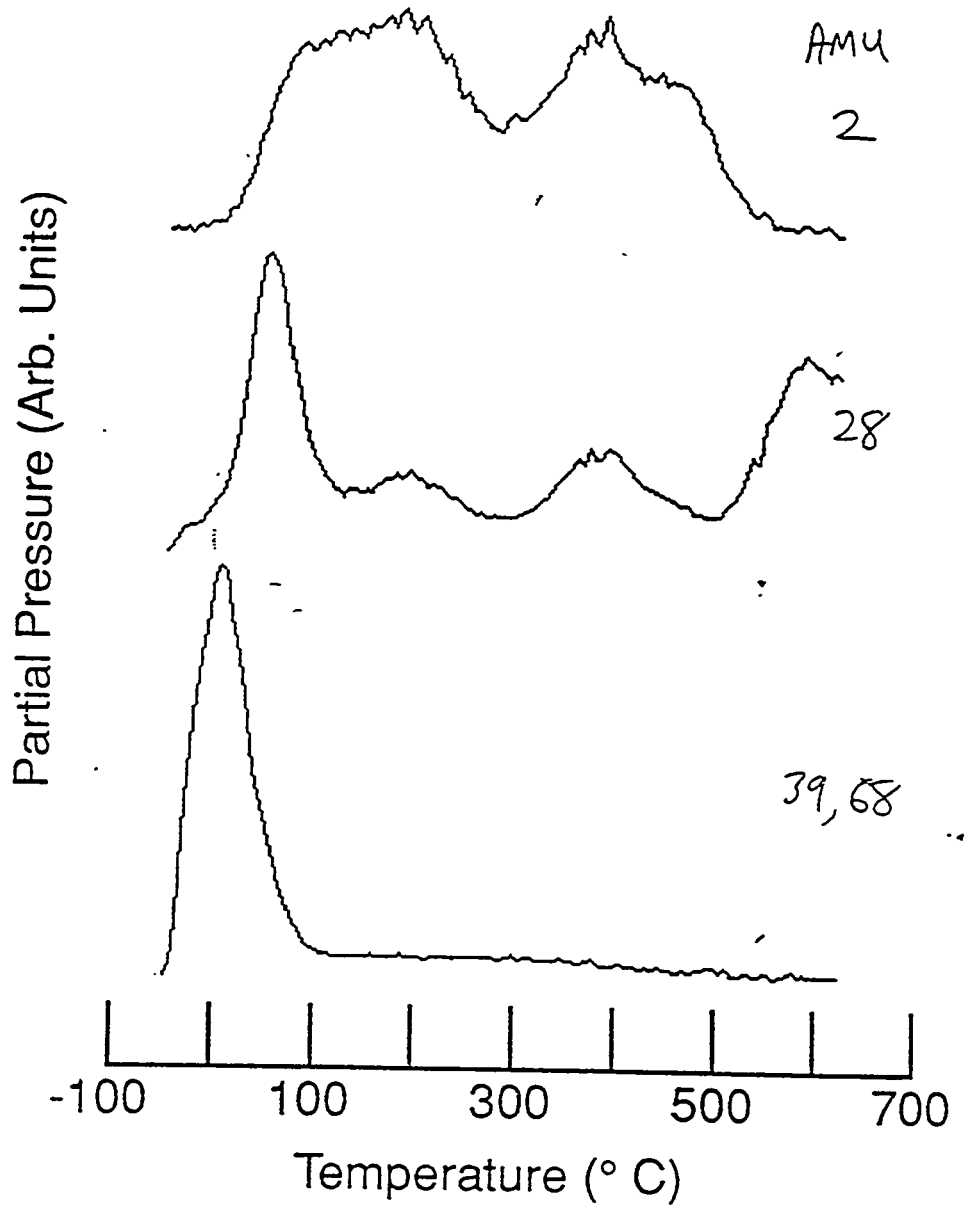

The TPRS spectrum from a saturation furan dose (about 0.5L) on a Mo(100) surface containing approximately 0.2ML of adsorbed sulfur (Fig. 5.3) reveals significant signals at m/e values of 68, 39, 28 and 2. The 39 and 68 AMU signals are the dominant cracking fraction and parent peaks from furan itself and hence the 39 and 68 AMU peaks seen near 275K are due to the desorption of molecularly adsorbed furan. The 2 AMU signal is quite similar to reports of the H_2 TPRS spectrum from thiophene/Mo(100) [1-3]. We assign the lowest temperature 2 AMU peak to desorption of hydrogen already present on the surface i.e. it has been cracked off from furan. The higher temperature peak can be reasonably assigned to stepwise dehydrogenation of chemisorbed hydrocarbon intermediates after the dissociative adsorption of furan. The second set of features in the H_2 TPRS spectrum near 400°C progressively disappear as the surface is sulfided (Figure 5.4); at about 0.5ML coverage, furan adsorption is suppressed, again in a similar manner to that seen for thiophene. A plot of the hydrogen TPRS peak area, or the C/Mo AES ratio (Figure 5.5), shows that the effect is linear with S coverage, arguing for a geometrical blocking effect of furan adsorption.

The 28 AMU spectrum shows a low temperature peak at about 330K followed by two small peaks and a further peak that commences below 1000K and continues to above 1100K. These too are supressed by sulfur and eliminated at a coverage of 0.5 ML (Figure 5.6). Results from Mo(110) are broadly similar (Figures 5.7 and 5.8) A fragment of m/e 28 is not a significant cracking feature of the mass spectrum of furan and furthermore the low-temperature 28 AMU desorption peak commences at a temperature at which all of the molecularly adsorbed furan has already desorbed. Hence this 28 AMU signal most probably arises from the production of carbon monoxide or ethylene on the surface. A careful examination of masses corresponding to all of the possible cracking products from these materials showed that this entire spectrum is in fact attributable to CO desorption

Figure 5.4 Hydrogen TPRS spectra from a saturation dose (0.5L) of furan on Mo(100) as a function of sulfur coverage.

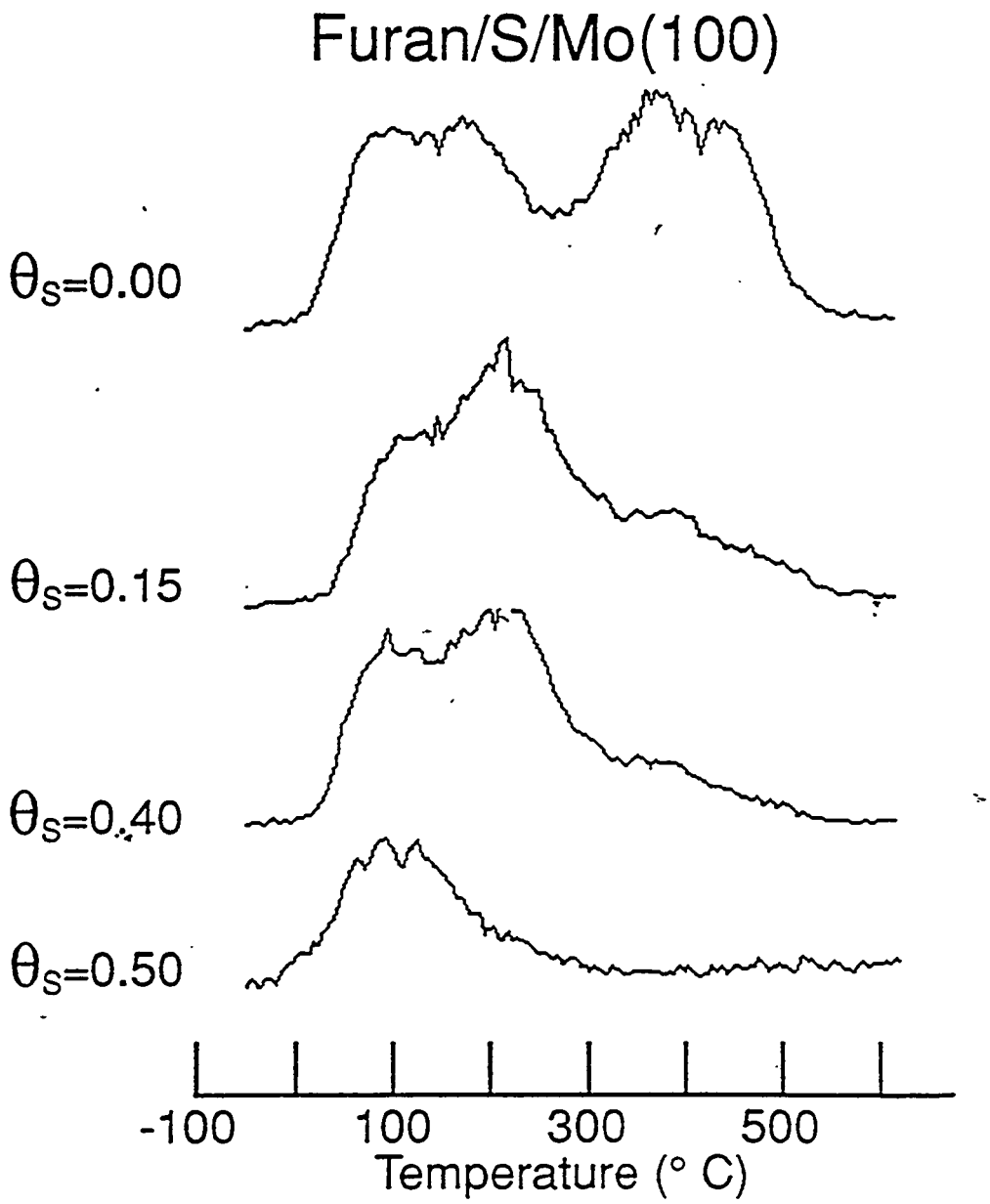

Figure 5.5 Blocking effect on furan adsorption as measured by hydrogen TPRS of C/Mo AES ratio

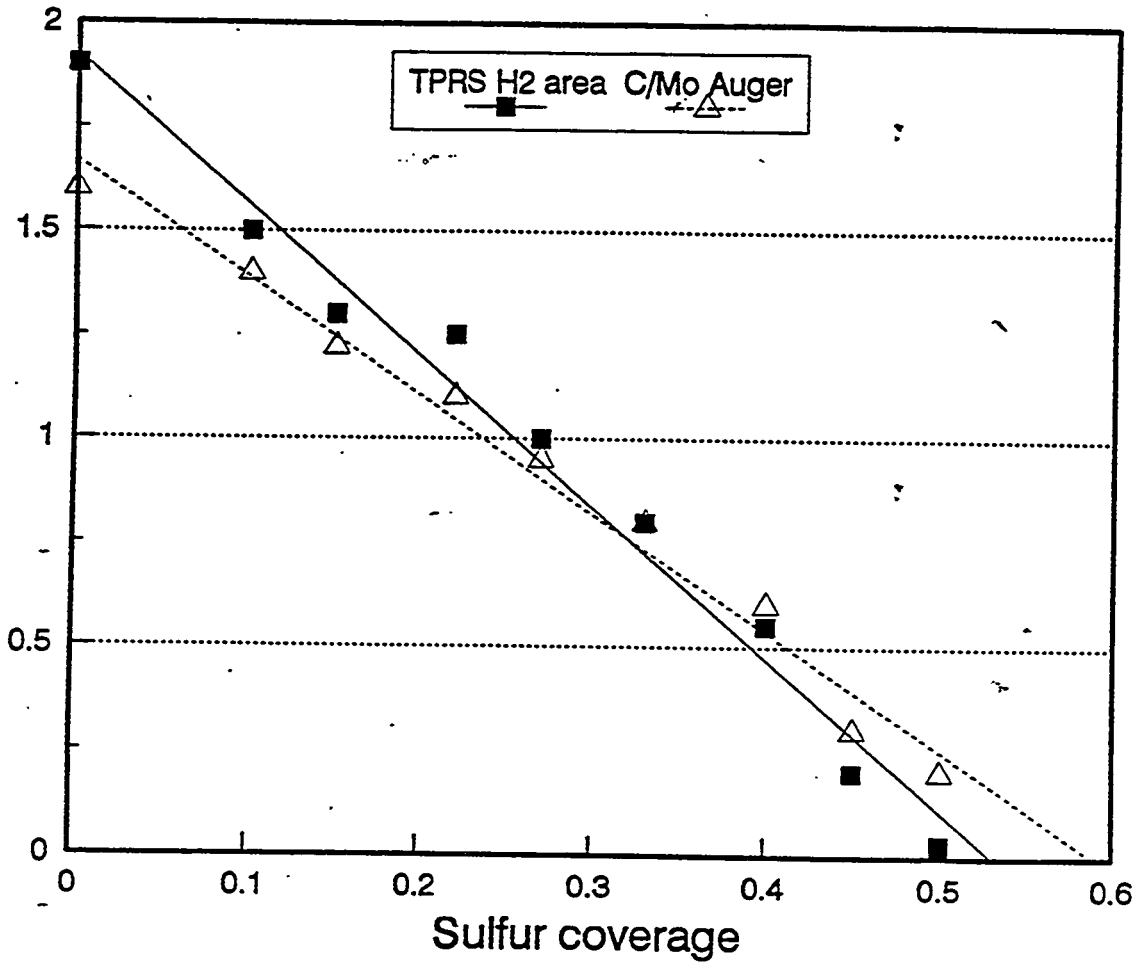

Figure 5.6 CO TPRS spectra from a saturation dose (0.5L) of furan on Mo(100) as a function of sulfur coverage.

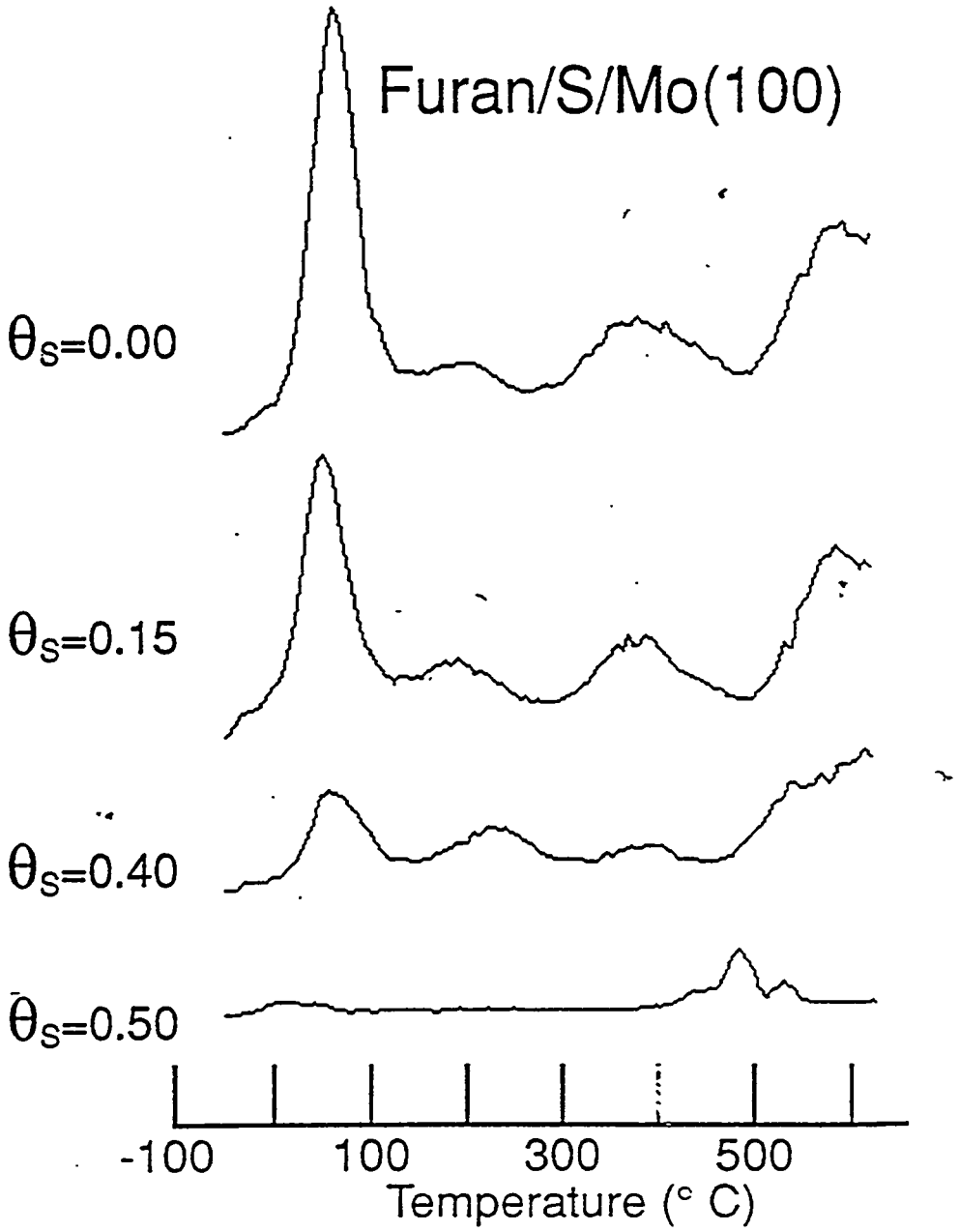

Figure 5.7 Hydrogen TPRS spectra from a saturation dose (0.5L) of furan on Mo(110) as a function of sulfur coverage.

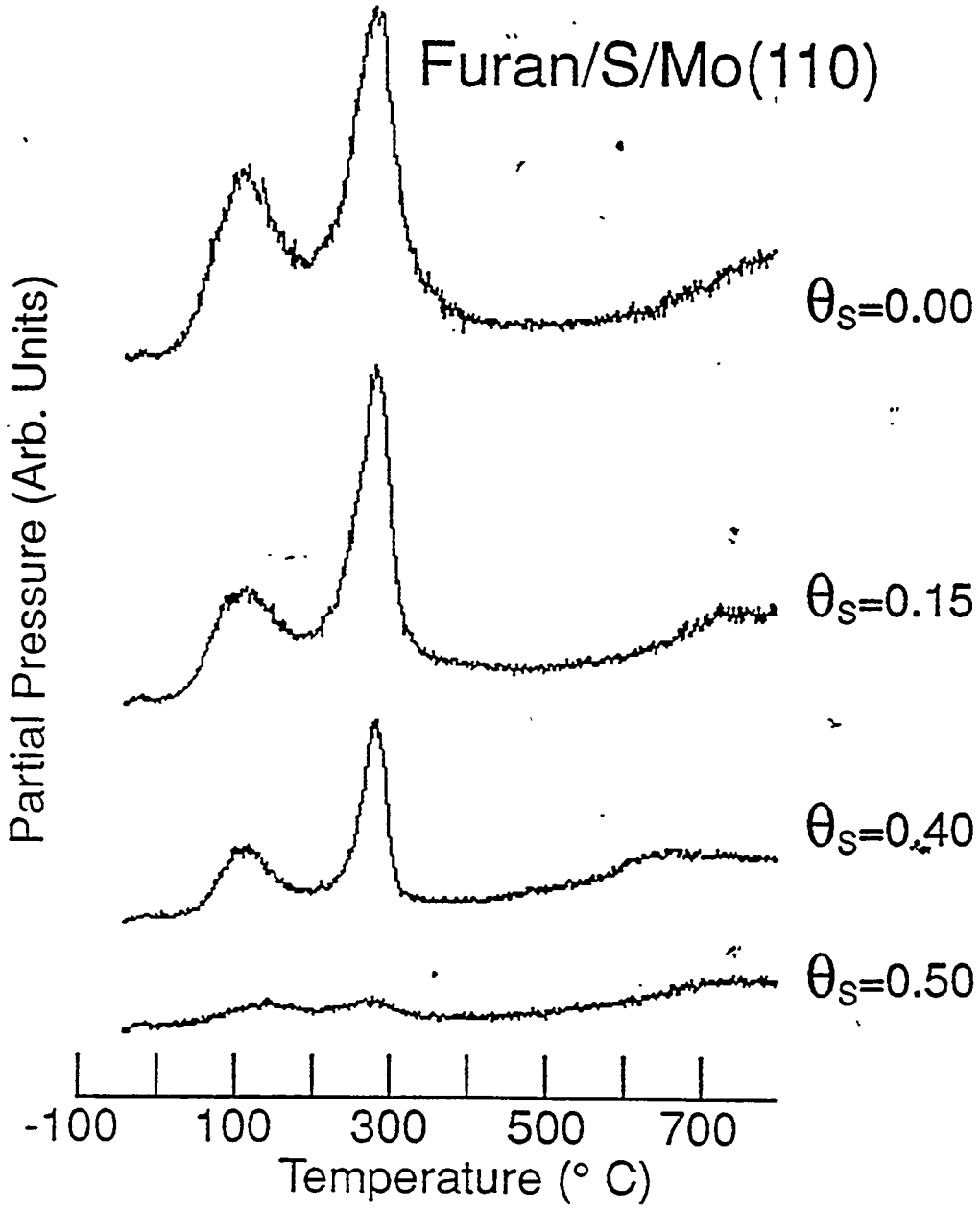

Figure 5.8 CO TPRS spectra from a saturation dose (0.5L) of furan on Mo(110) as a function of sulfur coverage.

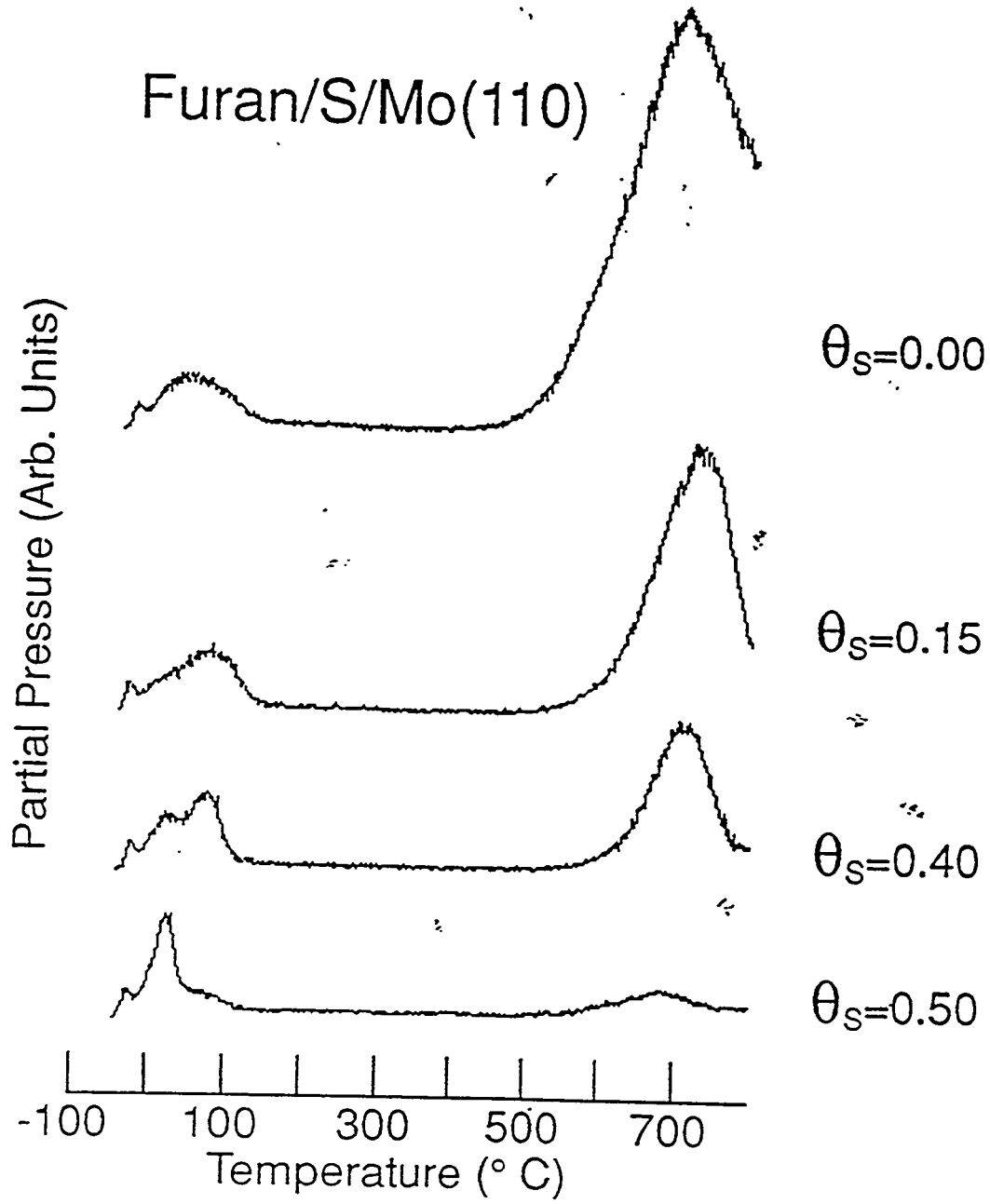

from adsorbed furan.

In Figure 5.9 we present similar data for the Mo(110) surface and compare it with the 28 AMU TPRS signal derived from the adsorption of CO itself. The latter spectrum shows two peaks. The low temperature peak only appears at high coverages of CO and has been attributed to first-order desorption of molecularly bound α-CO, whereas the high-temperature β peak is interpreted as a recombination of C and O atoms from dissociated CO [4,5]. Our CO/furan/Mo spectra also exhibit these two features at very similar desorption temperatures to those observed for adsorbed CO. An interesting difference between the two Mo surfaces is that two more small CO desorption peaks near 450K and 650K are present on the (100) surface, but not for (110). The similarity of the major 28 AMU peaks from furan adsorption to those seen from CO adsorption lead us to the conclusion that while a substantial amount of furan does indeed decompose to give atomic carbon and oxygen on the surface, which later desorbs as β-CO, a direct CO abstraction route also occurs at low temperatures close to 350K. The CO released from the furan molecule during this process is then immediately desorbed as it is above the normal α-CO desorption temperature (Figure 5.10)

We find support for this type of reaction chemistry in gas-phase pyrolysis experiments [6]. Here it is found that ring-opening of furan to form a stabilized biradical that subsequently decomposes into propyne and CO is a favored low energy reaction pathway (Figure 5.11). Such a mechanism may apply here to furan that has become bonded to the surface through loss of an α-H. However, the homogeneous reaction occurs at temperatures in excess of 1000K, whereas we observe the surface-mediated CO abstraction from furan close to room temperature.

This low-temperature direct abstraction of CO from furan, though a minority reaction on these surfaces, stands in contrast to the complete retention of sulfur from thiophene on the same surface.

Figure 5.9 CO and H_2 TPRS scans for a saturation (0.5L) dose of furan for 0.2ML of sulfur on Mo(100) and (110).

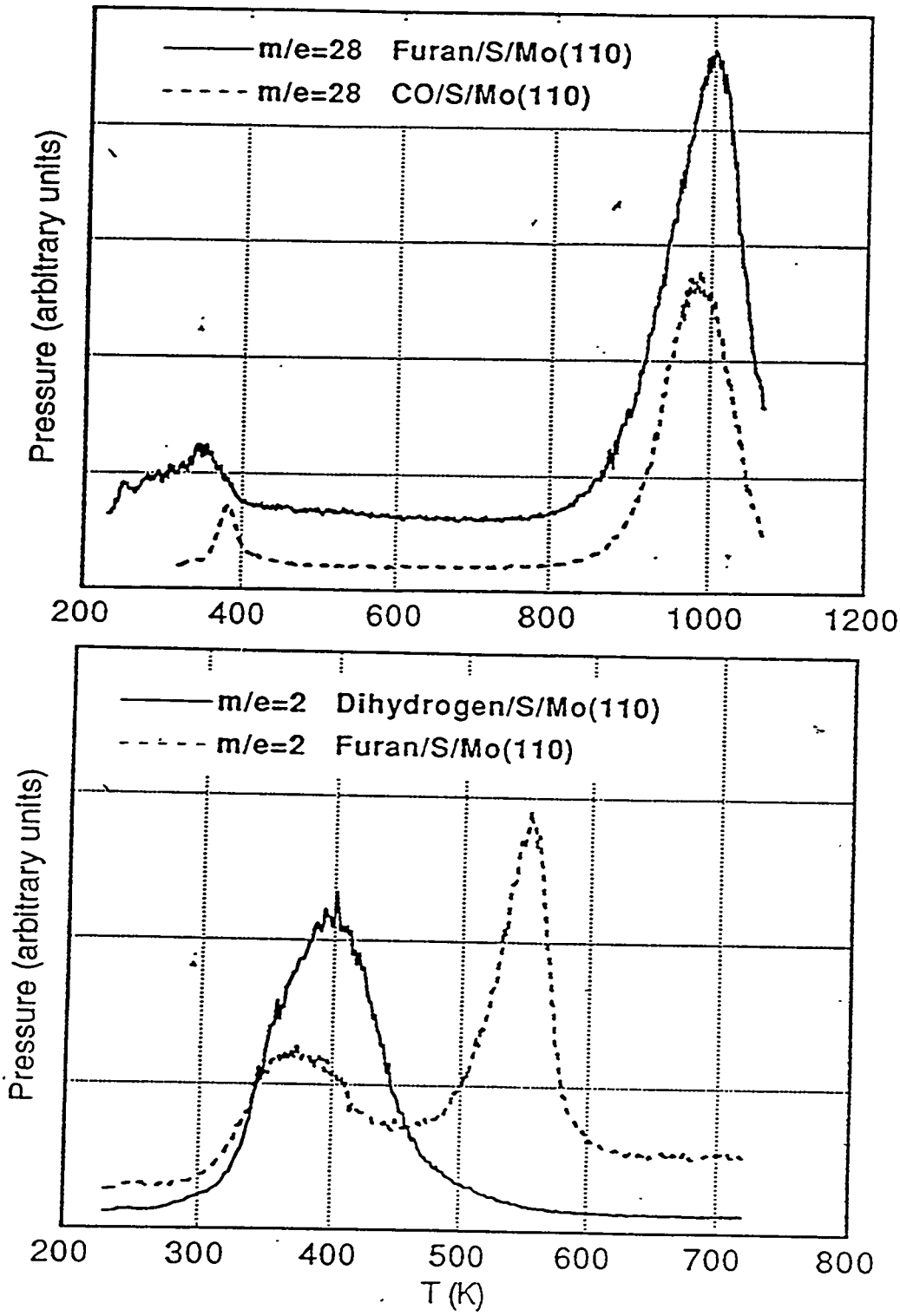

Figure 5.10 Reaction scheme for CO production from furan adsorption on sulfided Mo surfaces.

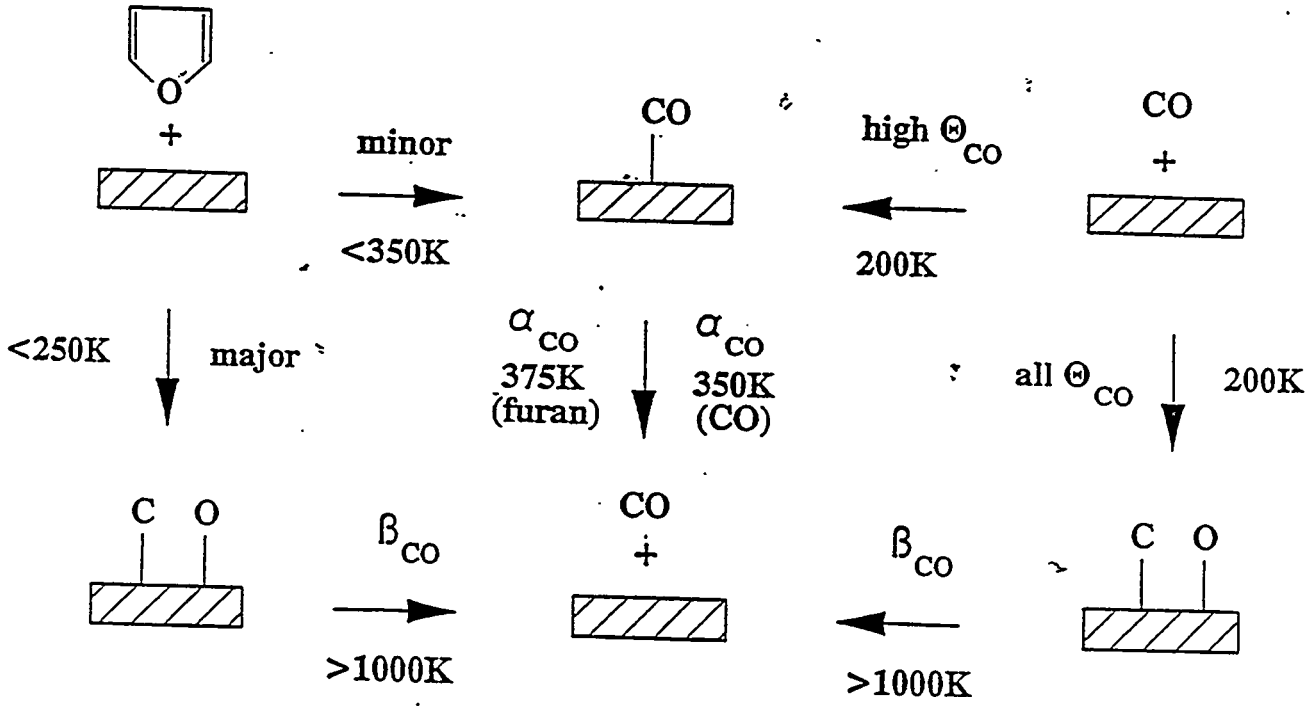

Figure 5.11 Reaction scheme for the gas-phase pyrolysis of furan [6]

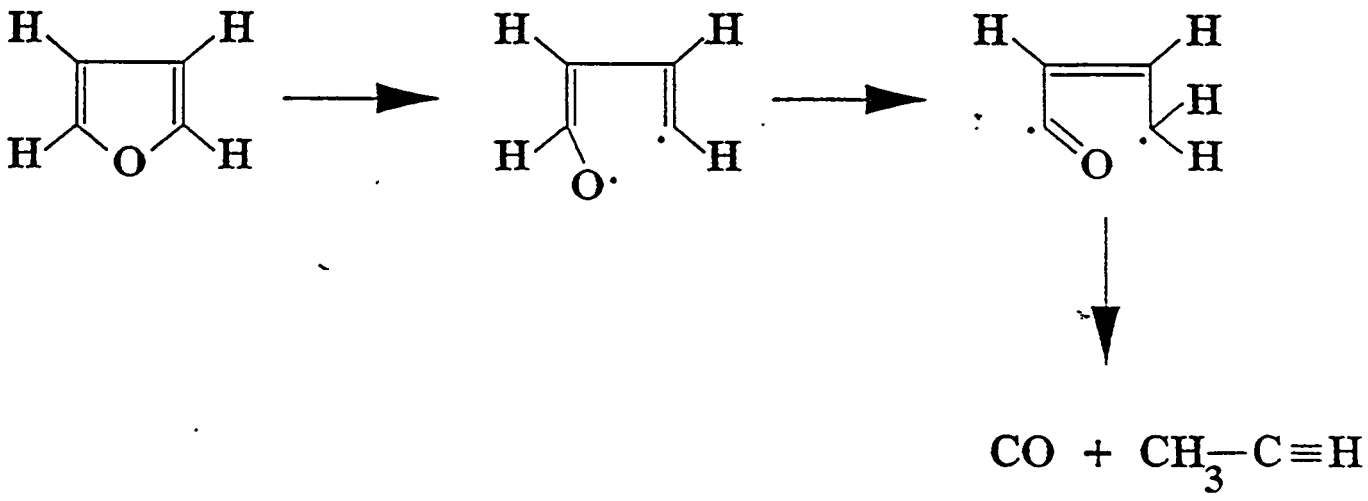

Though a suprising reaction at first sight, in hindsight the possibility of forming a stable gas-phase product in the case of furan, but not in the case of thiophene, provides an obvious driving force for this differing behavior.

Further evidence for these pathways comes from AES data. Both the intensity and the shape of the C Auger signal changes in synchrony with the TPRS data (Figures 5.12 and 5.13). During the course of a TPRS scan the shape of the C 283eV Auger changes from initially characteristic of C in a molecular environment, to finally a C signal characteristic of carbidic carbon. At intermediate temperatures a mixture of the two forms occurs. In addition the overall intensity of the C signal builds during the change from molecular to carbidic forms and eventually drops dramatically above 800C as the C dissolves into the bulk.

5.2 Reactions of furan on sulfided Mo(110) surfaces in the presence of hydrogen

HDO reactions of course use hydrogen to carry away the O in the heterocycle as water. Because the background pressure of hydrogen in the vacuum chamber is relatively high, it is sometimes convenient for our purposes to use deuterium rather than hydrogen itself. In order to model an HDO reaction in our system we can proceed in several ways:

i) pre- or coadsorb together with hydrogen with furan before starting a TDS ramp

ii) carry out a TDS ramp of a furan-dosed surface in a hydrogen (deuterium) atmosphere

iii) a combination of i) and ii)

We have in fact pursued all three of these possibilities using static hydrogen pressure of up to $5x10^{-7}$ torr. A large AMU 20 signal characteristic of D_2O appears in the chamber when D_2 is admitted that presumably arises from reaction with water on the chamber walls. This signal swamps any attempt to measure any D_2O production from any surface reaction. Hence we must concentrate

Figure 5.12 Changes in the intensity of the C Auger signal from adsorbed furan as a function of temperature.

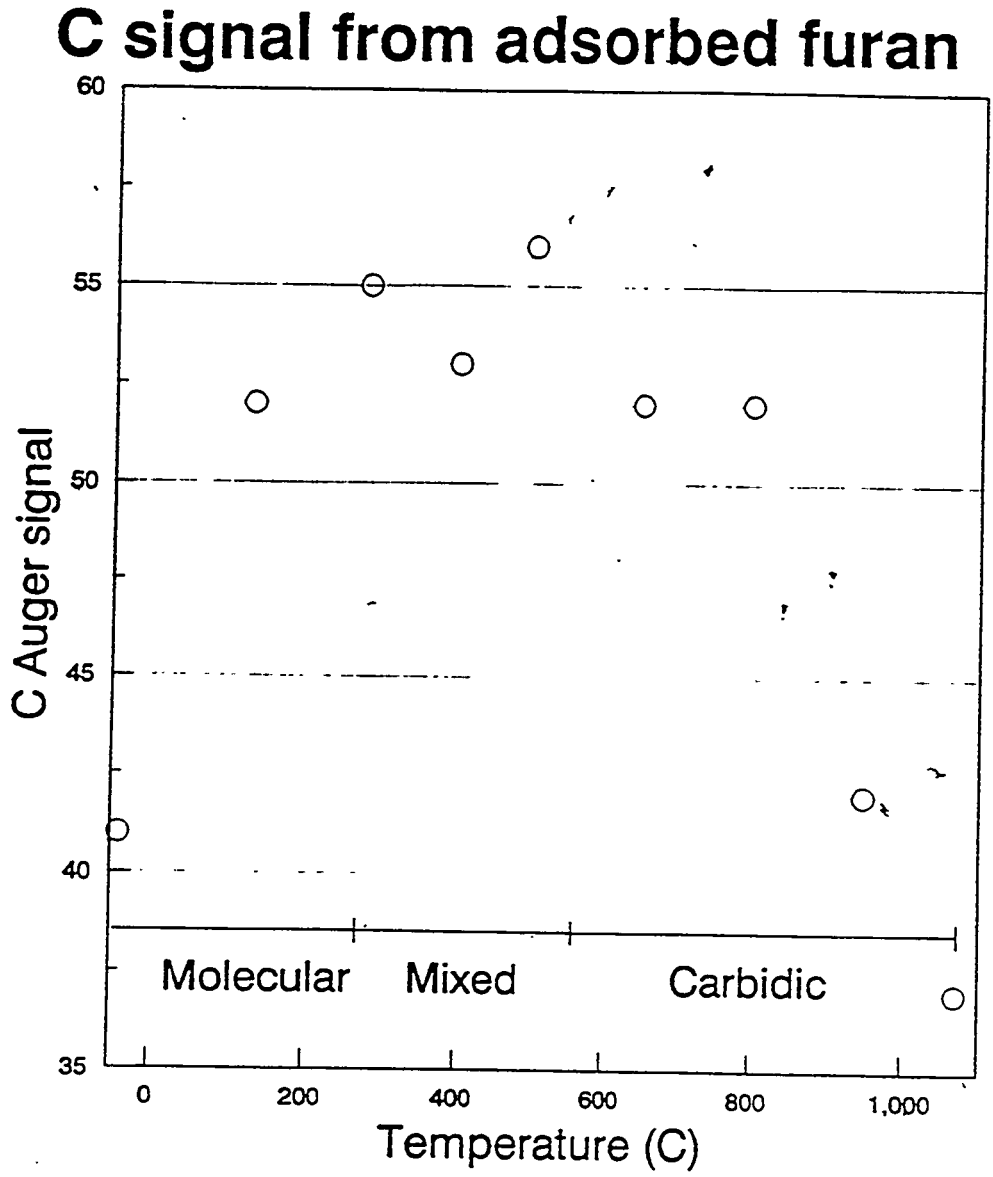

Figure 5.13 Variation of the shape of the C Auger signal from adsorbed furan as a function of temperature.

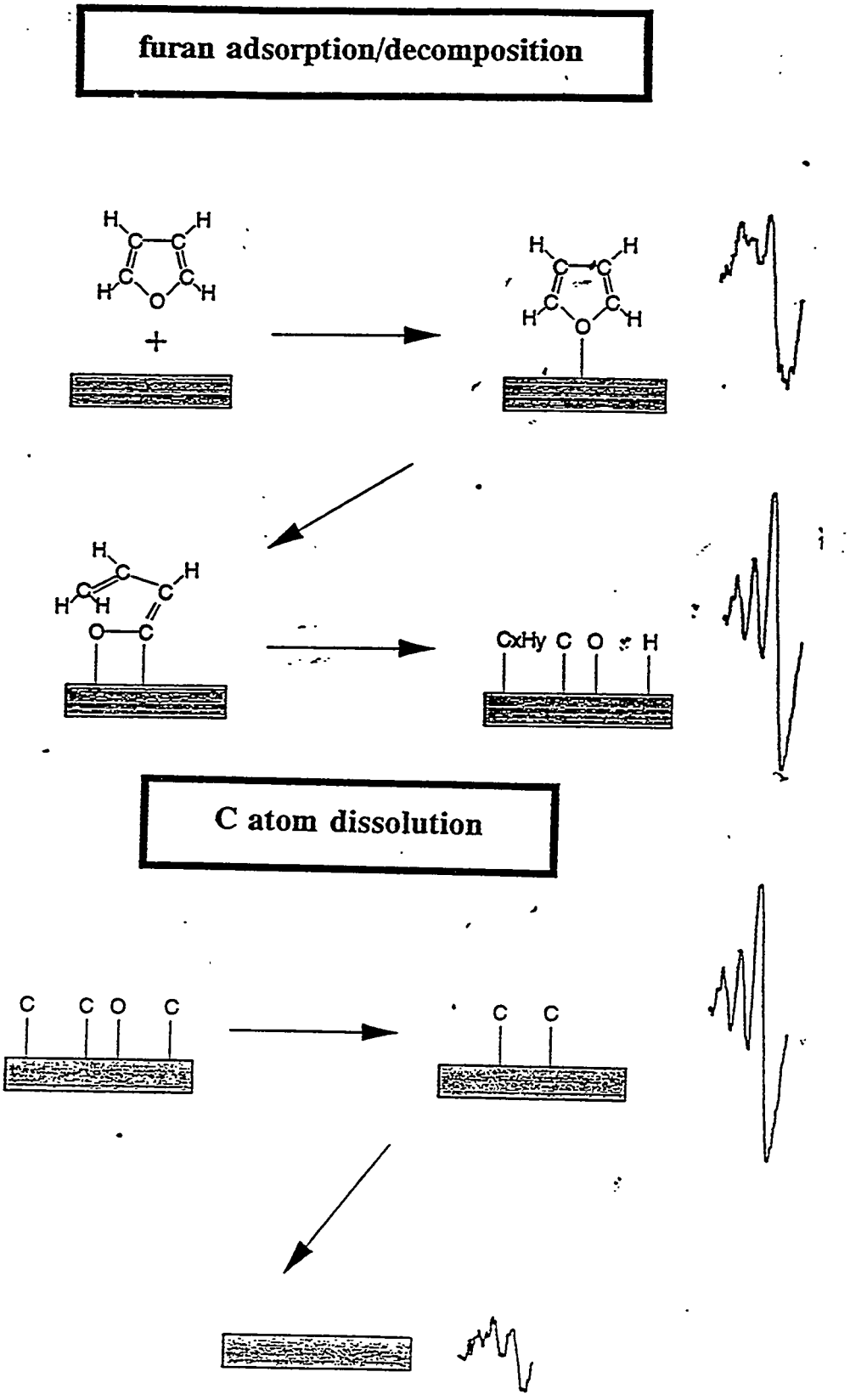

upon measurements of other potential HDO products (i.e. hydrocarbons) and spectroscopy of changes in surface composition. The sum of a large number of experiments indicates that we see only very small differences in the thermal reaction pathways of furan on sulfided Mo(110) regardless of whether D_2 is predosed and/or present during a thermal cycle. The type of path followed also does not vary in type with the sulfer coverage but does change in magnitude, being supressed above about 0.5 Ml coverage. Furan appears to decompose to a large extent on the surface even if hydrogen is initially present resulting in fragments that either desorb as CO or remain bonded to the surface as M-C or M-CH_x species.

5.3 Adsorption and reaction of substituted furans and tetrahydrofuran on Mo surfaces

Preliminary results from experiments carried out with substituted furans indicate that the pattern of reaction is very similar to that of furan itself. The most significant change appears to that substitution beyond the mono stage results in substantial blocking of the adsorption process.

5.4 References

1. M. Salmeron and G.A. Somorjai, Surf. Sci. 126, 410 (1983).
2. J.T. Roberts and C.M. Friend, J. Amer. Chem. Soc., 186 201 (1987).
3. F. Zaera, E.B. Kollin and J.L. Gland, Surf. Sci., 184, 75 (1987).
4. F. Zaera, E.B. Kollin and J.L. Gland, Chem. Phys. Lett.. 121, 464 (1985).
5. T.E. Felter and P.J. Estrup, Surf. Sci., 76, 464 (1978).
6. M.A. Grela, V.T. Amorebieta and A.J.Colussi, J.Phys. Chem., 89, 38 (1985).

6. Adsorption and reaction of hydrocarbons on Mo surfaces

Our experiments on furan adsorption show that reaction probably proceeds though dissociative adsorption followed by stepwise dehydrogenation of an adsorbed hydrocarbon intermediate. In order to shed more light on this process we have also investigated the adosrption and reaction of simple alkenes on sulfied Mo surfaces.

The series of experiments fall into two sets. The first examined the effect of varying the alkene gas dosage on the initially clean Mo(110) sample and the second used a saturation dose of each gas while varying the initial sulfur coverage on the sample. A typical experiment involves confirming sample cleanliness and predosing with sulfur if required. Then the gas of interest is leaked into the chamber via high precision valve; practical resolution for gas exposure using this equipment is $5x10^{-3}$ Langmuirs. At this point the TPRS run is initiated (0-400°C, 10°/sec.). Species monitored during the temperature ramp include dihydrogen and the parent molecule (or the principle cracking fragment of the parent). The latter provides a measure of how much, if any, of the dosed gas leaves the surface without decomposition. For hydrocarbons reacting over clean refractory metal surfaces extensive decomposition occurs; the H_2 TPRS curve area is a good qualitative measure of the number of gas molecules reacting [1]. The other indicator of the extent of decomposition, is the amount of residual carbon on the surface of the sample [2], which can be measured by AES. This carbon residue is measured at two different points during the experiment, immediately after the TPRS run and after a further heating to 850°C (to ensure complete decomposition). Subsequent data analysis yields integrated H_2 TPRS peak areas, H_2 peak maxima locations, and relative carbon coverage post reaction.

6.1 Hydrocarbon adsorption on clean Mo surfaces

Figure 6.1 shows plots of total integrated TPRS H_2 peak areas versus initial gas dosage for furan, ethylene, and propene on clean Mo(110). The shape of the curves for low exposures are very similar (Figure 6.1b), and the amount of H_2 evolved at saturation is similar for all three gases (Figure 6.1a). If total decomposition of the materials is occurring by the end of the temperature ramp at 400°C, then we would expect these areas to correlate with the amount of hydrogen available in the reactants. This correlation is approximately true for furan and ethylene, but the amount of hydrogen obtained from propene is only about 2/3 of that expected from total decomposition (Table 6.1). This could arise from either less propene molecules adsorbing, or imply that similar numbers of furan and ethylene molecules react while only 2/3 as many propene molecules decompose.

Figures 6.2 and 6.3 are analogous plots to Figure 6.1 which follows residual carbon deposits after heating to 400°C (Figure 6.2) or 850°C (Figure 6.3) as a function of gas dosage. Again the curves saturate at low exposures, but with differing amounts of surface carbon (see Table 6.1). The carbon residue is greatest for furan and is twice that from ethylene as would be expected if equal amounts of the two reactants had adsorbed. For propene the residual C AES signal is again about 2/3 of that expected for a molar amount adsorbed similar to that for ethylene or propene. The AES and TPRS data is therefore consistent with propene adsorption being hindered relative to either ethylene or furan.

Despite the apparent similarities between furan and ethylene reactions on clean Mo(110), the dehydrogenation processes for ethylene are energetically different from those of furan. As Table 6.1 indicates, the peak maximum for the release of hydrogen from the surface during a TPRS run is 100K higher for furan than for either hydrocarbon. Clearly, dehydrogenation of a hydrocarbon fragment

Figure 6.1 Total hydrogen TPRS areas from the adsorption of furan, ethylene and propene on Mo(110) a) for low doses and b) for high doses.

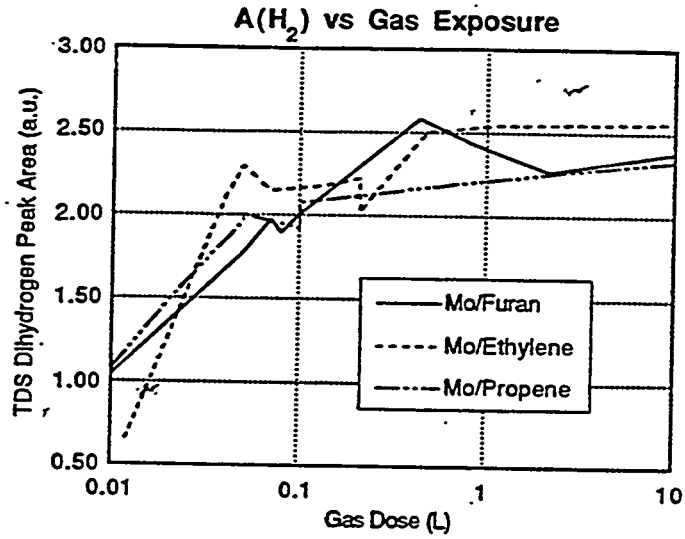

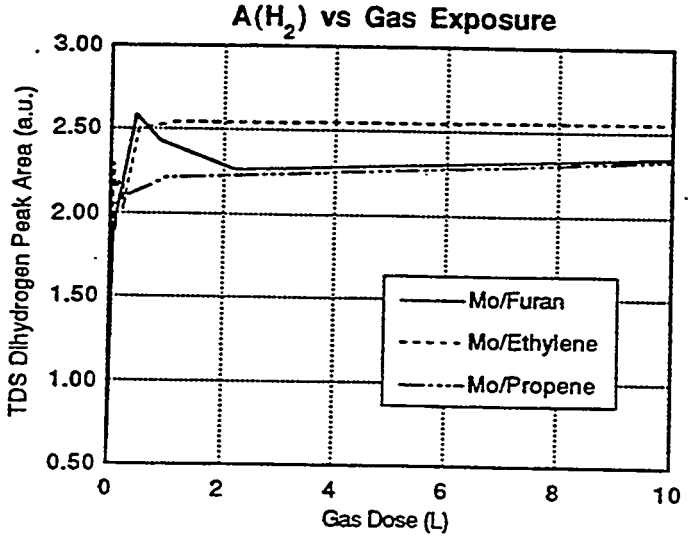

Figure 6.2 C/Mo AES ratio from the adsorption of furan, ethylene and propene on Mo(110) a) for low doses and b) for high doses at 400C.

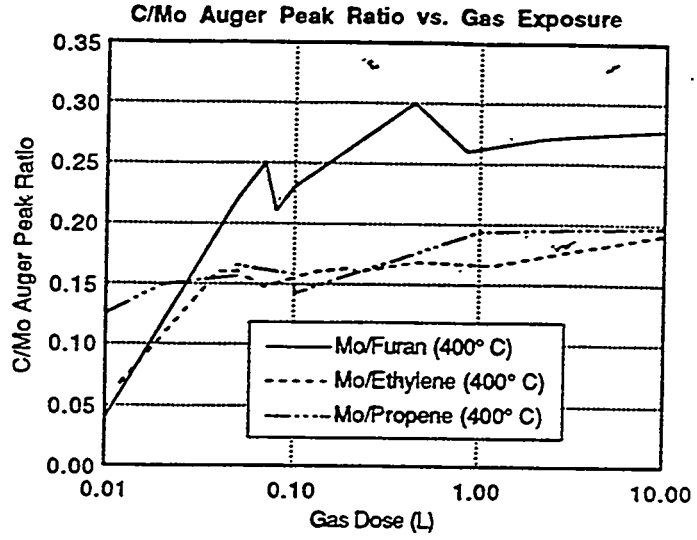

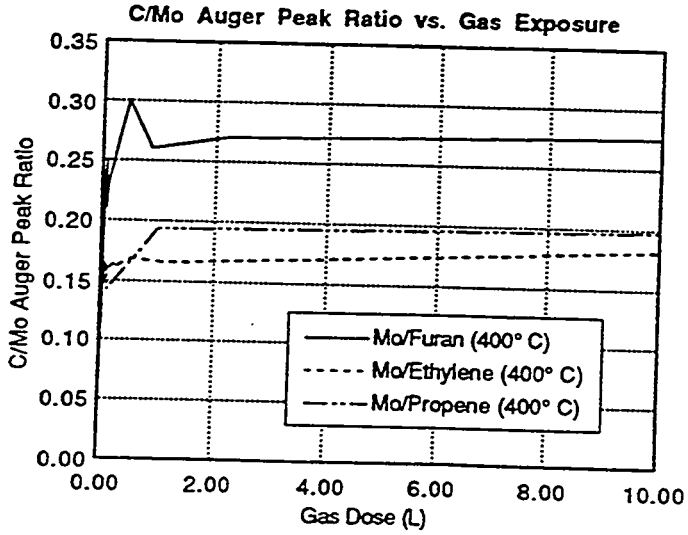

Figure 6.3 C/Mo AES ratio from the adsorption of furan, ethylene and propene on Mo(110) a) for low doses and b) for high doses at 850C.

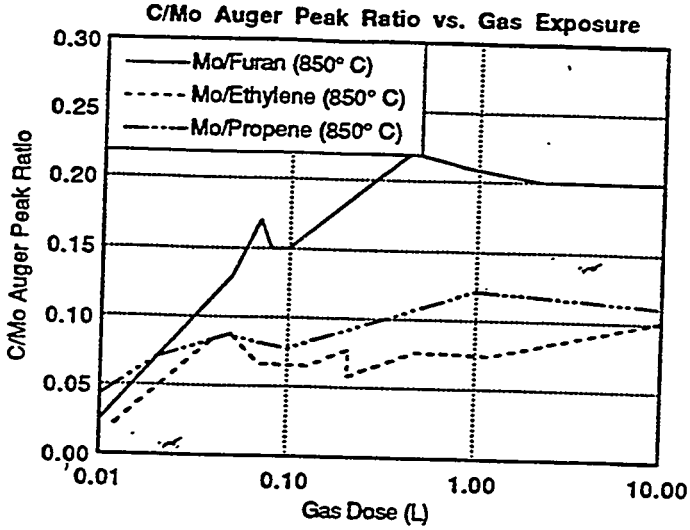

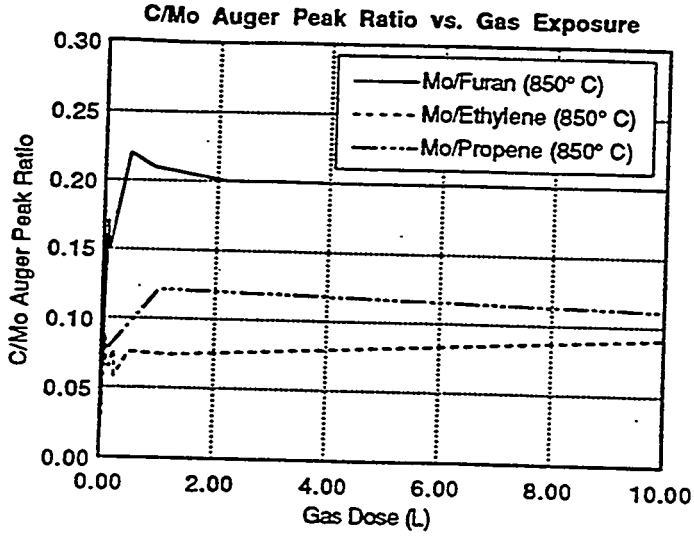

Table 6.1 Relative H_2 TPRS and C AES results for the adsorption of furan and hydrocarbons on clean Mo(110).

Adsorbate	Molecules H_2 available	H_2 TPRS Area (arbitrary units)	H_2 TPRS peak max.(K)	C atoms available	Relative C AES signal (400°C)	Relative C AE signal (850°C
Ethylene	2.0	2.5	430	2.0	1.8	0.9
Propene	3.0	2.3	420	3.0	2.0	1.1
Furan	2.0	2.3	530	4.0	2.7	2.0

from adsorbed furan is a higher energy process than the equivalent process for a simple hydrocarbon.

6.2 Adsorption of hydrocarbons on sulfided Mo surfaces

The second set of experiments held the gas dosages constant at a saturation value while varying the extent to which the Mo(110) is precovered with sulfur. Figure 6.4 shows the change in H_2 production as the sulfur precoverage is increased. The area of the TPRS curves are quite similar for each gas. The carbon residue AES measurements at 400 or 850°C for sulfur-covered Mo(110) from all three gas reactions were essentially indistinguishable (Figures 6.5 and 6.6). The marked differences between furan and ethylene H_2 TPRS areas and the much larger residual C present after furan adsorption on the clean surface are no longer apparent. The sulfur present on the surface appears to lower the amount of furan that will react. Both the TPRS and AES curves vary linearly with the amount of sulfur on the surface. This is consistent with an adsorption site blocking role for preadsorbed S. On Mo(100) sulfur is believed to cause little chemical modification of the surface; it mainly serves to physically block adsorption sites [1].

It is evident from this data is that a S/Mo AES peak ratio of 2.0 approaches the point at which gas reaction/absorption stops. A ratio of about 2.5 indicates 0.5 monolayers of sulfur using our equipment. With a sulfur coverage at or above 0.5 monolayers, no reaction is detectable by either TPRS or AES for all three gases. This implies that each of these gases requires two adjacent sites for decomposition since 0.5 ML of sulfur blocks 1 out of every 2 sites.

6.3 References

1. D.G. Kelly, Ph.D. Thesis, Univ. California, Berkeley, (1987).
2. J. Schwarz, Surf. Sci. 87 525 (1979).

Figure 6.4 Total hydrogen TPRS area as a function of sulfur coverage.

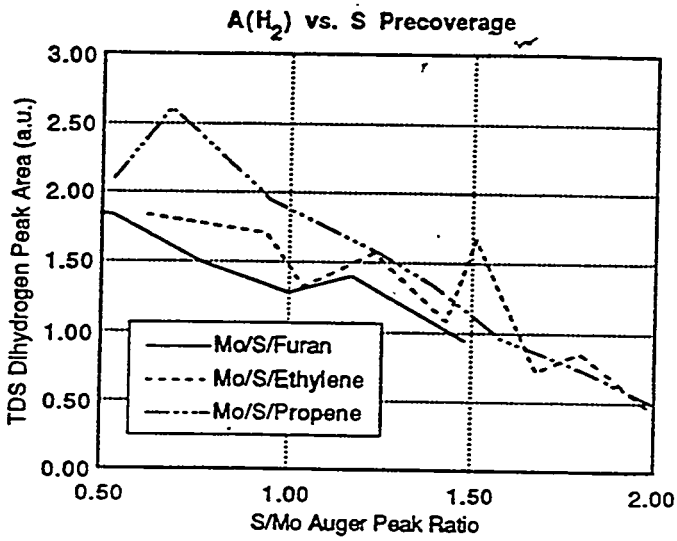

Figure 6.5 C/Mo AES ratio as a function of sulfur coverage at 400C.

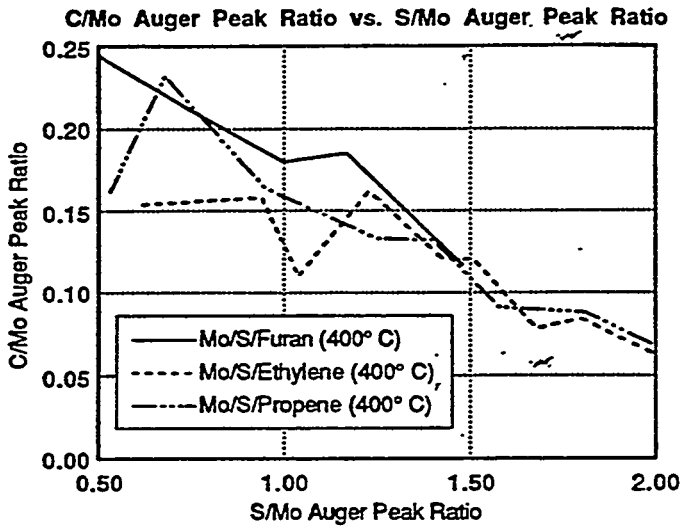

Figure 6.6 C/Mo AES ratio as a function of sulfur coverage at 850C.

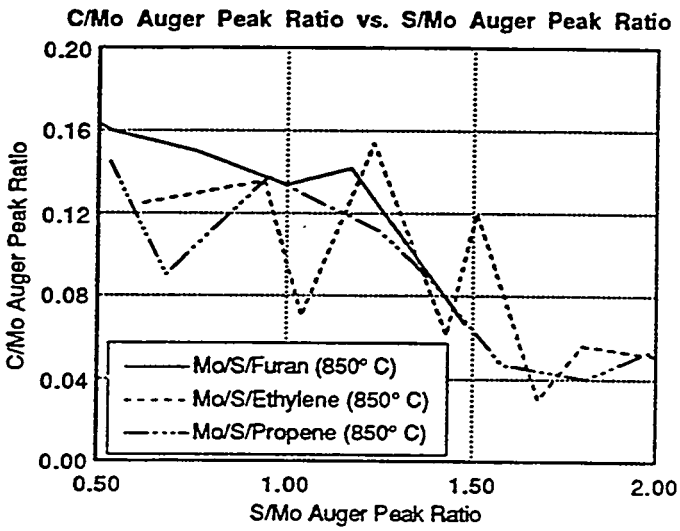

7. Summary

We now understand the reaction chemistry of furan on model sulfided Mo catalysts in some detail. Above a S/Mo ratio of about 0.5 ML, furan does not adsorb on sulfided Mo surfaces; as the sulfur coverage is lowered increasing amounts of furan can be adsorbed. Temperature-programmed reaction spectroscopy (TPRS) reveals that C-H, C-C and C-O bond scission occurs on these surfaces. Auger spectra show characteristic changes in the nature and amount of surface carbon. Comparisons with experiments carried out with CO, H_2 and alkenes show that reaction pathways include - direct abstraction of CO at low temperatures; cracking and release of hydrogen below its normal desorption temperature; dehydrogenation of adsorbed hydrocarbon fragments; recombination of C and O atoms and dissolution of carbon into the bulk at high temperatures. Performing the adsorption or thermal reaction in 10^{-5} torr of hydrogen does not change the mode of reaction significantly.

Principal findings:

- adsorption of furan is blocked by S; suppressed for S/Mo > 0.5 ML
- the principal reactions of furan on sulfided Mo surfaces are:
  - C-O scission and dehydrogenation of adsorbed hydrocarbon fragments
  - C-C bond scission and direct abstraction of molecular CO
  - recombination/desorption of C and O atoms as CO, and dissolution of C
- reaction in 10^{-5} torr of hydrogen does not change the mode of reaction significantly.

The results outlined above show that it is difficult to achieve true HDO reactions on sulfided Mo surfaces under the conditions we have used to date. Furan decomposition appears to dominate under all conditions. We can speculate on scenarios that may account for the lack of observed HDO

activity. The first is that the pressures we are using are simply too low; if we could operate at higher $H(D)_2$ partial pressures then hydrogenation may precede decomposition, resulting in HDO.

The second possibility is that the surface model we are using is incorrect, and the true active surface is yet to be found. We can find guidance in this area from experience in other areas of catalysis. In particular it is clear in Pt-catalyzed reforming reactions that the chemistry is taking place in a carbonaceous layer with ill-defined CH_x stoichiometry. This layer acts both as a buffer between reactants and metal, but more importantly can function either as a hydrogen sink or source. Perhaps the same situation occurs here. We know that the first adsorption of furan results in the deposition of carbon that is difficult to remove without also removing surface sulfur. Thus it could well be that a mixed $C/S/H_x$ surface layer is in fact important in HDO-type processes. Certainly it would not be possible to distinguish this sort of situation on the surface of the true catalyst unless the composition of the surface can be probed under operating conditions.